Structural optimization for frictionless contact

Sjövall, Filip

2025

Document Version:
Publisher's PDF, also known as Version of record

LUND UNIVERSITY

STRUCTURAL OPTIMIZATION FOR FRICTIONLESS CONTACT

FILIP SJÖVALL

Solid Mechanics

Doctoral Thesis

Structural optimization for frictionless contact

Filip Sjövall

LUND
UNIVERSITY

Akademisk avhandling som för avläggande av teknologie doktorsexamen vid tekniska fakulteten vid Lunds universitet kommer att offentligen försvaras fredagen den 23:e januari 2026 klockan 9.00 i sal M:E, M-huset, Ole Römers väg 1, Lund.
Fakultetsopponent: Prof. Pierre Duysinx, University of Liege, Belgien

Doctoral thesis which by due permission of the Faculty of Engineering at Lund University, will be publicly defended on 23rd of January 2026 at 9.00 a.m. in room M:E of the M-building, Ole Römers väg 1, Lund, Sweden.
Faculty opponent: Prof. Pierre Duysinx, University of Liege, Belgium

Organization
LUND UNIVERSITY

Division of Solid Mechanics
Box 118
SE–221 00 LUND
Sweden

Document name
DOCTORAL DISSERTATION

Date of disputation
2026-01-23

Sponsoring organization

Author(s)
Filip Sjövall

Title and subtitle
Structural optimization for frictionless contact

Abstract
Structural optimization aims to find the geometry of the best performing design in a predefined setting, using mathematical techniques. The motivation for this study can be categorized into three main benefits: efficient material usage, enhancing existing designs and enabling new technologies. All of these benefits are crucial for solving contemporary technological and environmental challenges.

An important topic of mechanical analysis is contact mechanics, which has been considered scarcely in structural optimization. Previous works have mainly considered linear elastic structures, often in contact with rigid supports, which limits the applicability to practical examples. The research herein investigates new structural optimization methodologies that combine state-of-the-art contact models with established optimization frameworks to develop methods capable of handling non-smooth contact interactions between deformable bodies. For this purpose, two contact models are investigated: the mortar method and the third medium contact method.

This thesis presents the underlying theory of frictionless contact, starting from the continuum formulation where both the mortar and third medium contact formulations are described as optimization problems. Numerical aspects of the contact modeling are discussed, after which the structural optimization framework is described. The proposed research methods are then presented in five appended papers.

Papers A and E explore the third medium contact model. In paper A the model is used to design metamaterials that can utilize internal contact using inverse homogenization and both shape and topology optimization. Paper E develops a new regularization method based on a rotation measure in the third medium that improves the efficacy of the model. In paper B, the mortar method is used to design axisymmetric structures for energy absorption using spline-based shape optimization. A "contact aware" shape optimization technique is developed in paper C which provides additional robustness to the optimization. This method is extended in paper D where the "contact aware" shape optimization is combined with topology optimization to provide additional design freedom.

Key words
Structural optimization, Contact mechanics, Finite strain, Shape optimization, Topology optimization, Mortar methods, Third medium contact.

Classification system and/or index terms (if any)

Supplementary bibliographical information

Language
English

ISSN and key title

ISBN
978-91-8104-751-6 (print)
978-91-8104-752-3 (pdf)

Recipient's notes

Number of pages
242

Price

Security classification

Department of Construction Sciences
Solid Mechanics

ISRN LUTFD2 /TFHF-25/1074-SE(1-242)
ISBN: 978-91-8104-751-6 (print)
ISBN: 978-91-8104-752-3 (pdf)

Structural optimization for frictionless contact

Doctoral Thesis by

Filip Sjövall

Printed by Media-Tryck AB, Lund, Sweden
For information, address:
Division of Solid Mechanics, Lund University, Box 118, SE-221 00 Lund, Sweden
Homepage: http://www.solid.lth.se

Preface

This thesis is the result of my time at the Division of Solid Mechanics, accompanied by many cups of coffee. It has been an amazing journey thanks to everyone who has been a part of it , and I would like to extend my gratitude to all of you. In particular, I have to thank my supervisor, Mathias Wallin, whose guidance and patience have been monumental to this work. I also have to give special thanks to the optimization group: Anna, Gunnar, Vilmer and Daniel whose company, both in and beyond our academic work, has been a constant source of enjoyment. Thanks also to all my current and former colleagues for your delightful company during our daily coffee breaks.

I am also thankful to all my friends whose obliviousness to stresses and strains has provided much needed distractions. Last but not least, the support of my family and Sophia has been valuable beyond measure.

Abstract

Structural optimization aims to find the geometry of the best performing design in a predefined setting, using mathematical techniques. The motivation for this study can be categorized into three main benefits: efficient material usage, enhancing existing designs and enabling new technologies. All of these benefits are crucial for solving contemporary technological and environmental challenges.

An important topic of mechanical analysis is contact mechanics, which has been considered scarcely in structural optimization. Previous works have mainly considered linear elastic structures, often in contact with rigid supports, which limits the applicability to practical examples. The research herein investigates new structural optimization methodologies that combine state-of-the-art contact models with established optimization frameworks to develop methods capable of handling non-smooth contact interactions between deformable bodies. For this purpose, two contact models are investigated: the mortar method and the third medium contact method.

This thesis presents the underlying theory of frictionless contact, starting from the continuum formulation where both the mortar and third medium contact formulations are described as optimization problems. Numerical aspects of the contact modeling are discussed, after which the structural optimization framework is described. The proposed research methods are then presented in five appended papers.

Papers A and E explore the third medium contact model. In paper A the model is used to design metamaterials that can utilize internal contact using inverse homogenization and both shape and topology optimization. Paper E develops a new regularization method based on a rotation measure in the third medium that improves the efficacy of the model. In paper B, the mortar method is used to design axisymmetric structures for energy absorption using spline-based shape optimization. A "contact aware" shape optimization technique is developed in paper C which provides additional robustness to the optimization. This method is extended in paper D where the "contact aware" shape optimization is combined with topology optimization to provide additional design freedom.

Popular Scientific Summary

Efficient material usage is essential in manufacturing processes for maximizing profit and minimizing environmental impact. Given a set of desired attributes in a design, structural optimization finds the geometry that maximizes these attributes. Typically, desired attributes are strong and durable structures of minimal weight, but other physical properties are possible.

This thesis develops new structural optimization methods for the design of structures that are strongly influenced by contact interactions. Contact is important in many areas of engineering such as manufacturing processes, lubrication, brakes, sealing structures and crashworthiness, to name a few. Accurate contact models that can be harnessed in engineering design is therefore crucial for improving existing designs and developing new technologies. Unfortunately, the mathematical treatment of contact mechanics is difficult. When two bodies come in contact and deform due to external loading it is hard to determine the shape and size of the contact zone over which they interact. Since the advent of numerical techniques, the field of contact mechanics has solved increasingly complex problems. In spite of contact algorithms becoming more sophisticated, many difficulties of contact mechanics still pose a challenge for structural optimization methods. This is because structural optimization is based on numerical simulations, so the difficulty of the numerical treatment of contact mechanics is inherited. Because of this, past research in structural optimization has to a large extent been focused on small deformations and contact with rigid bodies. Large deformation contact problems have begun to attract interest, although research in this area remains limited.

This thesis develops methods that combine state of the art gradient based structural optimization with modern algorithms in contact mechanics to enable new possibilities for designing structures in frictionless contact that can experience large deformations. Two main methods for contact modeling are explored. The first, called the *mortar* method, is a widely used method that models contact in an average sense, which is useful because the numerical treatment of contact involves faceted geometries as a result of the discrete nature of computer modeling. The second, called the *third medium* contact method, utilizes a fictitious medium between contacting bodies to transfer contact forces. This method has the advantage of treating the contact constraints implicitly so that the cumbersome work of relating discrete contact surfaces to each other is avoided. Both methods are combined with prominent structural optimization methods and showcased for several applications.

Populärvetenskaplig sammanfattning

Effektiv materialanvändning är avgörande i tillverkningsprocesser för att maximera vinst och minimera miljöpåverkan. Givet en uppsättning önskade egenskaper i en konstruktion finner strukturoptimering den geometri som maximerar dessa egenskaper. Typiskt sett utgörs de önskade egenskaperna av starka och hållfasta strukturer med minimal vikt, men även andra fysikaliska egenskaper är möjliga.

Denna avhandling utvecklar nya metoder för strukturoptimering vid utformning av konstruktioner som är starkt påverkade av kontaktinteraktioner. Kontakt spelar en viktig roll inom många områden av ingenjörsvetenskapen, såsom tillverkningsprocesser, smörjning, bromsar, tätningsstrukturer och krocksäkerhet, för att nämna några. Noggranna kontaktmodeller som kan utnyttjas i beräkningsbaserad konstruktion är därför avgörande för att förbättra befintliga konstruktioner och utveckla ny teknik. Dessvärre är den matematiska behandlingen av kontaktmekanik komplicerad. När två kroppar kommer i kontakt och deformeras på grund av yttre belastning är det svårt att bestämma formen och storleken på den kontaktzon över vilken de interagerar. Sedan numeriska metoder introducerades har området kontaktmekanik kunnat hantera alltmer komplexa problem. Trots att kontaktalgoritmer har blivit mer sofistikerade utgör många av kontaktmekanikens svårigheter fortfarande en utmaning för strukturoptimeringsmetoder. Detta beror på att strukturoptimering baseras på numeriska simuleringar, och svårigheterna i den numeriska behandlingen av kontaktmekanik därmed överförs. På grund av detta har tidigare forskning inom strukturoptimering till stor del fokuserat på små deformationer och kontakt med stela kroppar. Kontaktproblem med stora deformationer har under senare år uppmärksammats men området är fortfarande relativt outforskat.

Denna avhandling utvecklar metoder som kombinerar den senaste gradientbaserade strukturoptimeringen med moderna algoritmer inom kontaktmekanik, för att möjliggöra nya tillvägagångssätt för att utforma strukturer i friktionsfri kontakt som kan genomgå stora deformationer. Två huvudsakliga metoder för kontaktmodellering undersöks. Den första, kallad *mortar* metoden, är en allmänt använd metod som modellerar kontakt i en genomsnittlig bemärkelse, vilket är användbart eftersom den numeriska behandlingen av kontakt behandlar fasetterade geometrier till följd av den diskreta naturen hos datorbaserad modellering. Den andra, kallad *third medium*-metoden, använder ett fiktivt medium mellan kropparna i kontakt för att överföra kontaktkrafter. Denna metod har fördelen att kontaktvillkoren behandlas implicit, vilket gör att det besvärliga arbetet med att koppla samman diskreta kontaktytor kan undvikas. Båda metoderna kombineras med framstående strukturoptimeringsmetoder och demonstreras för flera olika tillämpningar.

List of appended papers

This doctoral thesis is based on the following manuscripts:

Paper A
Anna Dalklint, Filip Sjövall, Mathias Wallin, Seth Watts and Daniel Tortorelli
Computational design of metamaterials with self contact
Computer Methods in Applied Mechanics and Engineering, 417 (2023): 116424

Paper B
Filip Sjövall, Mathias Wallin and Daniel Tortorelli
Shape optimization of hyperelastic structures subject to frictionless contact
Computers & Structures, 301 (2024): 107426

Paper C
Filip Sjövall and Mathias Wallin
A contact aware regularization technique for shape optimization
Computational Mechanics, (2025): 1-17.

Paper D
Filip Sjövall and Mathias Wallin
Shape and topology optimization for contact applications
Under review.

Paper E
Vilmer Dahlberg, Filip Sjövall, Anna Dalklint and Mathias Wallin
A rotation-based approach to third medium contact regularization
Under review.

Own Contribution
The author has taken the main responsibility in the preparation and writing of papers B, C and D. In papers A and E the development of the numerical model, preparation of the manuscript and analysis was performed in collaboration with the co-authors.

Contents

Chapter 1

Introduction

Structural optimization is the subject of using mathematical optimization to design structures that carry load. The idea is to find the best, or a better, performing structure with respect to a desired measure denoted *objective* under a predefined set of restrictions denoted *constraints*. To measure the performance, a model for the physical behavior is required, and, a relation between this model and the design geometry has to be established.

The physical behavior is commonly modeled using partial differential equations (PDEs) that are solved with the finite element method, which will be the case herein. In this thesis, the design is related to the numerical model via its geometric features using topology and shape optimization. Topology optimization aims to distribute material in an optimal way whereas shape optimization alters the boundaries of a design without nucleating holes. While shape optimization is more restrictive, it offers benefits in terms of boundary resolution.

Numerical structural optimization saw its rise as the finite element method became popular. An early approach was node-based shape optimization (Zienkiewicz and Campbell, 1973) and soon thereafter shape optimization using various boundary representations, such as splines (Braibant and Fleury, 1984) were proposed, see Haftka and Grandhi (1986) for an early review. Homogenization methods for topology optimization were presented in Bendsøe and Kikuchi (1988) and soon thereafter, density-based methods using material penalization (Bendsøe, 1989; Rozvany et al., 1992) became popular. Level-set based methods (Sethian and Wiegmann, 2000; Osher and Santosa, 2001) have also become popular, and have been used for both shape and topology optimization (Allaire et al., 2002; Wang et al., 2003). Other shape optimization methods have also been developed and filtering techniques (Azegami and Wu, 1996; Hojjat

et al., 2014) have improved node-based approaches. Spline representations have become more sophisticated and are used as an alternative to the finite element method in isogeometric analysis (Hughes et al., 2005). Additionally, level-set methods, using for instance XFEM to resolve the material boundary (Sukumar et al., 2001; Duysinx et al., 2006) have been developed. Research has also been devoted to combining shape and topology optimization (Bletzinger and Maute, 1997).

While most early works employed linear elastic material models, modern structural optimization research has evolved to include many complex physical phenomena such as: stress constraints (Yang and Chen, 1996; Duysinx and Bendsøe, 1998; Holmberg et al., 2013), plasticity (Maute et al., 1998; Wallin et al., 2016), heat transfer (Gersborg-Hansen et al., 2006; Dbouk, 2017), aerodynamics (Kennedy and Martins, 2014) and acoustics (Wadbro and Berggren, 2006; Yoon et al., 2007) to highlight a few examples. Advancements have also been made in the realm of large scale computing (Borrvall and Petersson, 2001; Schmidt and Schulz, 2011), and a plethora of educational software for topology optimization have been published (Wang et al., 2021).

The topic of this thesis is structural optimization methods for applications including contact mechanics. Although contact is present on many scales, the work herein is exclusively focused on frictionless contact at the macroscale using continuum models. Contact is present in almost all mechanical interactions and is vital in many engineering applications like for example gears, brakes and manufacturing processes. The contact interaction between two deformable bodies is difficult to model due to the fact that the contact interface is unknown beforehand and since the bodies are separate the interaction is inherently *discontinuous*. Additionally, the spatial discretization of the contact surfaces introduces faceted boundaries that may not conform. Despite these challenges, modern numerical methods are able to handle complex contact scenarios. Classically, numerical contact mechanics has been handled by enforcing the contact constraints on numerical grids via the *node-to-node*, *node-to-segment* and *segment-to-segment* methods (Wriggers and Laursen, 2006). A common feature for the aforementioned methods is that they all relate the contacting grids explicitly, and as such, require search algorithms when the contact interface is changing. The *third medium contact* method avoids this procedure by utilizing an intermediate fictitious material to translate contact forces between two bodies. This method recently gained attention (Bluhm et al., 2021; Frederiksen et al., 2024) as density-based topology optimization already makes use of a fictitious medium in the form of the void material. While promising, this method relies on excessive deformations of the fictitious material which makes it prone to numerical issues related to distorted elements in the third medium.

Following the development of numerical contact algorithms, many studies have con-

sidered structural optimization of contacting structures. Since the works of Klarbring et al. (1995) optimizing trusses in contact, several studies have considered contact in topology optimization (Fancello, 2006; Strömberg and Klarbring, 2010; Bruggi and Duysinx, 2013), and shape optimization (Hilding et al., 2001; Beremlijski et al., 2002). Until recently, most research have considered linear elastic structures, often utilizing contact with rigid supports. Nevertheless, several works have considered large deformations (Lawry and Maute, 2018) and also friction (Stupkiewicz et al., 2010). Formulations that can handle non-conforming grids using the *mortar method* have also been of interest (Strömberg, 2017; Fernandez et al., 2020; Sjövall et al., 2024; Sjövall and Wallin, 2025). Likewise, the third medium contact approach has been combined with topology optimization to design mechanisms in the large-deformation regime (Bluhm et al., 2021), metamaterials with tailored macroscopic properties (Dalklint et al., 2023) and thermo-mechanical regulators (Dalklint et al., 2025). Recently, a 499-line MATLAB code for topology optimization with friction was published (Wang et al., 2025).

The objective of the research herein is to develop methods that combine modern contact methods with shape and topology optimization. The mortar method, which is a *segment-to-segment* type method that models contact between two bodies in the weak sense is combined with shape and topology optimization. This formulation provides several benefits for the optimization, which is showcased in papers B, C and D. The less conventional *third medium contact* method is utilized in paper A for the design of metamaterials and a new regularization technique for third medium contact modeling is developed in paper E.

Chapter 2

Continuum model

The theory in this thesis is based on continuum mechanics and to establish the framework that will be used for the contact formulation, this chapter reviews the necessary concepts. In particular, the kinematical description and material model are presented.

2.1 Kinematics

Consider the body $\mathcal{B}$ that initially resides in its *reference configuration* Ω with particles described by the reference coordinates $\boldsymbol{X}_0$. Assuming quasi-static conditions, $\mathcal{B}$ is displaced by $\boldsymbol{u}(\boldsymbol{X})$ into its *current configuration* ω with particles described by the spatial coordinates $\boldsymbol{x} = \boldsymbol{X} + \boldsymbol{u}(\boldsymbol{X})$. The gradient of $\boldsymbol{x}$ with respect to the reference

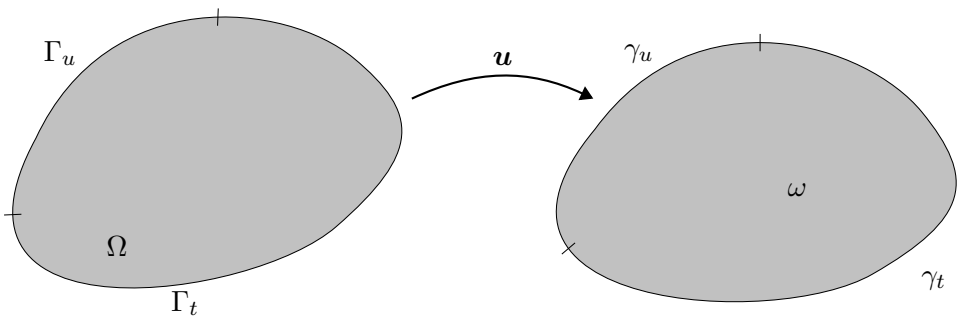

Figure 2.1: Continuum kinematics.

coordinates $\boldsymbol{X}$ is denoted the *deformation gradient* $\boldsymbol{F}$, that is,

$$\boldsymbol{F} = \frac{\partial \boldsymbol{x}}{\partial \boldsymbol{X}} = \boldsymbol{I} + \nabla \boldsymbol{u}, \tag{2.1}$$

where $\boldsymbol{I}$ is the second order identity tensor. The deformation gradient measures the deformation locally and describes the mapping from line elements $d\boldsymbol{X}$ in Ω to line elements $d\boldsymbol{x}$ in ω such that

$$d\boldsymbol{x} = \boldsymbol{F} d\boldsymbol{X}. \tag{2.2}$$

The mapping (2.2) is assumed to be unique, necessitating the constraint

$$J = \det \boldsymbol{F} > 0, \tag{2.3}$$

where J is the Jacobian that measures the transformation of volume elements, i.e.

$$dv = J dV. \tag{2.4}$$

Using the polar decomposition, $\boldsymbol{F}$ is split into

$$\boldsymbol{F} = \boldsymbol{R}\boldsymbol{U}, \tag{2.5}$$

where $\boldsymbol{R}$ is the *rotation tensor* while $\boldsymbol{U}$ is the positive definite symmetric *right stretch tensor*. The deformation gradient $\boldsymbol{F}$ is also used to define strain measures like the Green-Lagrange strain tensor

$$\boldsymbol{E} = \frac{1}{2}(\boldsymbol{C} - \boldsymbol{I}), \tag{2.6}$$

where $\boldsymbol{C} = \boldsymbol{F}^T \boldsymbol{F}$.

2.2 Governing equation

The potential Π due to the stored elastic energy in $\mathcal{B}$, the *surface tractions* $\bar{\boldsymbol{T}}$ on Γ_t and the *body forces* $\boldsymbol{B}$ is described by the functional

$$\Pi(\boldsymbol{u}) = \int_\Omega W(\boldsymbol{F}) d\Omega - \int_\Omega \boldsymbol{B} \cdot \boldsymbol{u} d\Omega - \int_{\Gamma_t} \bar{\boldsymbol{T}} \cdot \boldsymbol{u} d\Gamma. \tag{2.7}$$

Given the prescribed displacement $\boldsymbol{u} = \bar{\boldsymbol{u}}$ on Γ_u, the equilibrium configuration of $\mathcal{B}$ is found when the potential Π is stationary. This corresponds to a minimization of the potential and the solution is found by requiring that the variation of Π with respect to $\boldsymbol{u}$ vanishes, whereby

$$\delta\Pi(\boldsymbol{u}, \delta\boldsymbol{u}) = \int_\Omega \frac{\partial W}{\partial \boldsymbol{F}} : \delta \boldsymbol{F} d\Omega - \int_\Omega \boldsymbol{B} \cdot \delta\boldsymbol{u} d\Omega - \int_{\Gamma_t} \bar{\boldsymbol{T}} \cdot \delta\boldsymbol{u} d\Gamma = 0, \tag{2.8}$$

where the arbitrary virtual displacements $\delta\boldsymbol{u}$ must satisfy $\delta\boldsymbol{u} = \boldsymbol{0}$ on Γ_u. The boundaries Γ_u and Γ_t are denoted γ_u and γ_t in the current configuration.

2.3 Constitutive model

The work herein models materials using hyperelasticity, which is based on the assumption that there exists a *strain-energy function* W per unit volume, from which a relation between stresses and strains can be derived. If the analysis is restricted to mechanical loads, this function can be expressed using $\boldsymbol{F}$. The *first Piola-Kirchhoff* stress tensor $\boldsymbol{P}$ is then obtained from

$$\boldsymbol{P} = \frac{\partial W(\boldsymbol{F})}{\partial \boldsymbol{F}}. \tag{2.9}$$

By construction, the energy should fulfill

$$W(\boldsymbol{F}) \geq 0, \tag{2.10}$$

meaning that the energy should increase with deformation and for rigid body motions $\boldsymbol{F} = \boldsymbol{I}$ or pure rotations $\boldsymbol{F} = \boldsymbol{R}$ the energy should be zero, i.e.

$$W(\boldsymbol{I}) = W(\boldsymbol{R}) = 0, \tag{2.11}$$

The energy W should tend to infinity when the material is compressed such that its volume approaches zero

$$W(\boldsymbol{F}) \to \infty \quad \text{as} \quad J \to 0, \tag{2.12}$$

which is called a *growth condition* (Holzapfel, 2002).

Herein, compressible neo-Hookean material models have been utilized (Simo and Pister, 1984), that is

$$W(\boldsymbol{F}) = \frac{K}{2}(J^2 - 1 - \ln(J)) + \frac{G}{2}(J^{-2/3}\text{tr}(\boldsymbol{F}^T\boldsymbol{F}) - \boldsymbol{I}). \tag{2.13}$$

The strain energy (2.13), consists of two parts: the first is related to volumetric deformations scaled by the *bulk modulus* K while the second part relates to *distortional* deformations scaled by the *shear modulus* G. Importantly, the bulk part contains the $\ln J$-term which fulfills (2.12). Considering isotropic materials in the small strain limit, K and G can be expressed in terms of the Young's modulus E and Poisson's ratio ν via

$$K = \frac{E}{3(1-2\nu)}, \quad G = \frac{E}{2(1+\nu)}. \tag{2.14}$$

Chapter 3

Contact mechanics

To model contact interactions, a description of the kinematics of the potential contact surfaces is required. When contact between two bodies occurs, the bodies are prohibited from penetrating each other and the minimization of $\Pi(\boldsymbol{u})$ must include a *non-penetration constraint*. The result is a constrained optimization problem, for which there are several solution methods. To remain consistent with the appended papers the formulation is limited to 2D. The corresponding formulation in 3D can be found in e.g. Puso and Laursen (2004); Wriggers and Laursen (2006).

3.1 Minimum distance

To establish the contact kinematics, consider the two bodies $\mathcal{B}_1$ and $\mathcal{B}_2$ with potential contact surfaces of $\gamma_c^{(1)}$ and $\gamma_c^{(2)}$, on the deformed configurations $\omega^{(1)}$ and $\omega^{(2)}$, respectively. To quantify their state of contact, it will be useful to parameterize $\gamma^{(2)}$ using the coordinate ζ; see Fig. 3.2. Once the bodies are loaded, they may come into contact, and to determine their contact state, their proximity is measured by the distance between a point $\boldsymbol{x}^{(1)}$ on $\gamma_c^{(1)}$ and a point $\boldsymbol{x}^{(2)}(\zeta)$ on $\gamma_c^{(2)}$ via

$$r(\zeta) = ||\boldsymbol{x}^{(1)} - \boldsymbol{x}^{(2)}(\zeta)||_2. \tag{3.1}$$

The point on $\gamma_c^{(2)}$ closest to $\boldsymbol{x}^{(1)}$ is the minimizer of (3.1) with respect to ζ that follows from

$$\left.\frac{dr}{d\zeta}\right|_{\zeta=\bar{\zeta}} = \frac{\boldsymbol{x}^{(1)} - \boldsymbol{x}^{(2)}(\bar{\zeta})}{||\boldsymbol{x}^{(1)} - \boldsymbol{x}^{(2)}(\bar{\zeta})||_2} \cdot \boldsymbol{\tau}^{(2)}(\bar{\zeta}) = 0, \tag{3.2}$$

where $\boldsymbol{\tau}^{(2)}(\bar{\zeta}) = \left.\frac{d\boldsymbol{x}^{(2)}}{d\zeta}\right|_{\zeta=\bar{\zeta}}$ is the tangent vector at $\bar{\zeta}$. The result of (3.2) is that the minimum distance from a point $\boldsymbol{x}^{(1)}$ to $\gamma^{(2)}$ requires that $\boldsymbol{x}^{(1)} - \boldsymbol{x}^{(2)}(\bar{\zeta})$ is orthogonal

to $\boldsymbol{\tau}^{(2)}(\bar{\zeta})$, wherefore the surface normal of $\gamma^{(2)}$ at $\bar{\zeta}$ is recovered from

$$\boldsymbol{n}^{(2)} = \frac{\boldsymbol{x}^{(1)} - \boldsymbol{x}^{(2)}(\bar{\zeta})}{||\boldsymbol{x}^{(1)} - \boldsymbol{x}^{(2)}(\bar{\zeta})||_2}. \tag{3.3}$$

The process of finding $\boldsymbol{x}^{(2)}(\bar{\zeta})$ from the solution of (3.2), is called the closest point projection. Although unlikely when contact occurs, (3.1) is not necessarily convex and (3.2) potentially has multiple solutions. This occurs when $\boldsymbol{x}^{(1)}$ is equally close to many points on $\gamma_c^{(2)}$, such as when $\boldsymbol{x}^{(1)}$ is located at the center of a circular cavity $\gamma^{(2)}$, however this is rare in practice.

3.2 Gap function

The state of contact between a point $\boldsymbol{x}^{(1)}$ and $\gamma^{(2)}$ is quantified using the closest point projection via the gap function g, defined as

$$g(\boldsymbol{u}) = (\boldsymbol{x}^{(1)} - \boldsymbol{x}^{(2)}(\bar{\zeta})) \cdot \boldsymbol{n}^{(2)}(\bar{\zeta}), \tag{3.4}$$

where $\boldsymbol{u} = (\boldsymbol{u}^{(1)}, \boldsymbol{u}^{(2)})$. Upon computing g, three states can be distinguished, as shown in Fig. 3.1. Penetration of the bodies occurs when $g < 0$ and is unphysical.

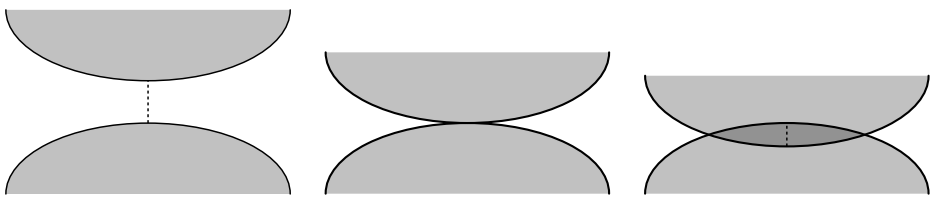

(a) Separation $g > 0$ (b) Contact $g = 0$ (c) Penetration $g < 0$

Figure 3.1: Gap function states.

Therefore, the *non-penetration constraint* is imposed as

$$g(\boldsymbol{u}) \geq 0. \tag{3.5}$$

An alternative definition of the gap function, g', makes use of the normal field $\boldsymbol{n}^{(1)}$ instead of $\boldsymbol{n}^{(2)}(\bar{\zeta})$. The second gap function g' is

$$g'(\boldsymbol{u}) = -(\boldsymbol{x}^{(1)} - \boldsymbol{x}^{(2)}(\hat{\zeta})) \cdot \boldsymbol{n}^{(1)}, \tag{3.6}$$

where $\boldsymbol{x}^{(2)}(\hat{\zeta})$ is the point on $\gamma^{(2)}$ that is intersected by the line emanating from $\boldsymbol{x}^{(1)}$ in the direction of $\boldsymbol{n}^{(1)}$. This gap function is suitable for segment-based *mortar*

methods (Yang et al., 2005). Both gap functions suffer from bias, as they might produce different values if the bodies are interchanged. An illustration of g and g' is presented in Fig. 3.2. While g measures proximity based on the exact solution of the closest point projection, g' enables a numerical treatment of the non-penetration constraint that uses a continuous normal field, so that there are no jumps in g' between element facets. Ultimately, $\boldsymbol{n}^{(1)}$ and $\boldsymbol{n}^{(2)}$ should coincide at the state of contact.

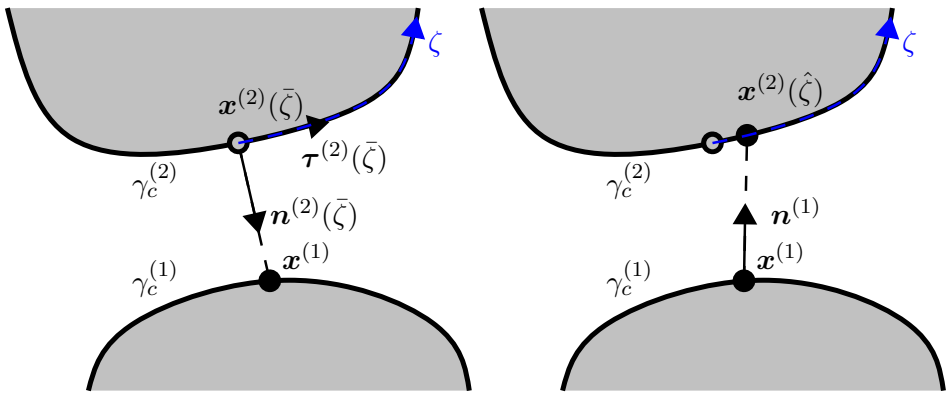

(a) Gap function g based on $\boldsymbol{n}^{(2)}$. (b) Gap function g' based on $\boldsymbol{n}^{(1)}$

Figure 3.2: Gap functions.

3.3 Normal contact

Having defined the gap function g, it is possible to classify the state of contact. However, not only the deformation of the contact surfaces is unknown beforehand, but also the forces acting upon them. In the absence of friction, the contact traction $\boldsymbol{t}_c^{(i)}$ on a potential contact boundary $\gamma_c^{(i)}$ can be expressed as $\boldsymbol{t}_c^{(i)} = \lambda \boldsymbol{n}^{(i)}$ where λ is the contact pressure and $\boldsymbol{n}^{(i)}$ is the normal to the surface. Assuming that there is no adhesion, $\boldsymbol{t}_c^{(i)}$ must be compressive or vanish, necessitating the constraint

$$\lambda \leq 0. \tag{3.7}$$

Furthermore, the contact pressure should only be non-zero when the gap is zero, or vice versa. This is the *complementary condition*

$$\lambda g(\boldsymbol{u}) = 0. \tag{3.8}$$

By combining (3.5), (3.7) and (3.8), the Hertz-Signorini-Moreau conditions are established as

$$g(\boldsymbol{u}) \geq 0, \qquad \lambda \leq 0, \qquad \lambda g(\boldsymbol{u}) = 0. \tag{3.9}$$

The conditions (3.9) are illustrated in Fig. 3.3 where the feasible domain is marked in red. Clearly, the non-smooth contact behavior is not differentiable at $g = 0$.

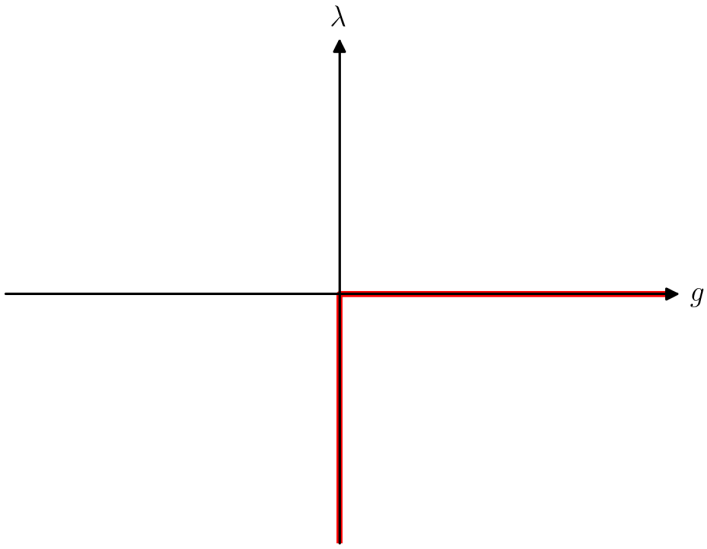

Figure 3.3: Visualization of the contact constraints (3.9).

3.3.1 Potential contact energy

The equilibrium configuration of two bodies $\mathcal{B}^{(1)}$ and $\mathcal{B}^{(2)}$ in frictionless contact corresponds to the following constrained minimization problem

$$\begin{aligned} &\min_{\boldsymbol{u}} \sum_{i=1}^{2} \Pi(\boldsymbol{u}^{(i)}), \\ &\text{subject to } g(\boldsymbol{u}) \geq 0 \text{ on } \gamma_c, \end{aligned} \tag{3.10}$$

where $\Pi(\boldsymbol{u}^{(i)})$ is the potential energy of body i and γ_c is the contact surface. The problem (3.10) can be recast by introducing the total potential energy Π_{tot} as

$$\Pi_{tot}(\boldsymbol{u}, \lambda) = \sum_{i=1}^{2} \Pi(\boldsymbol{u}^{(i)}) + \int_{\gamma_c} \lambda g(\boldsymbol{u}) d\gamma = \sum_{i=1}^{2} \Pi(\boldsymbol{u}^{(i)}) + \Pi_c(\boldsymbol{u}, \lambda), \tag{3.11}$$

for which it is possible to formulate the saddle point problem

$$\min_{\boldsymbol{u}} \max_{\lambda \leq 0} \Pi_{tot}(\boldsymbol{u}, \lambda). \tag{3.12}$$

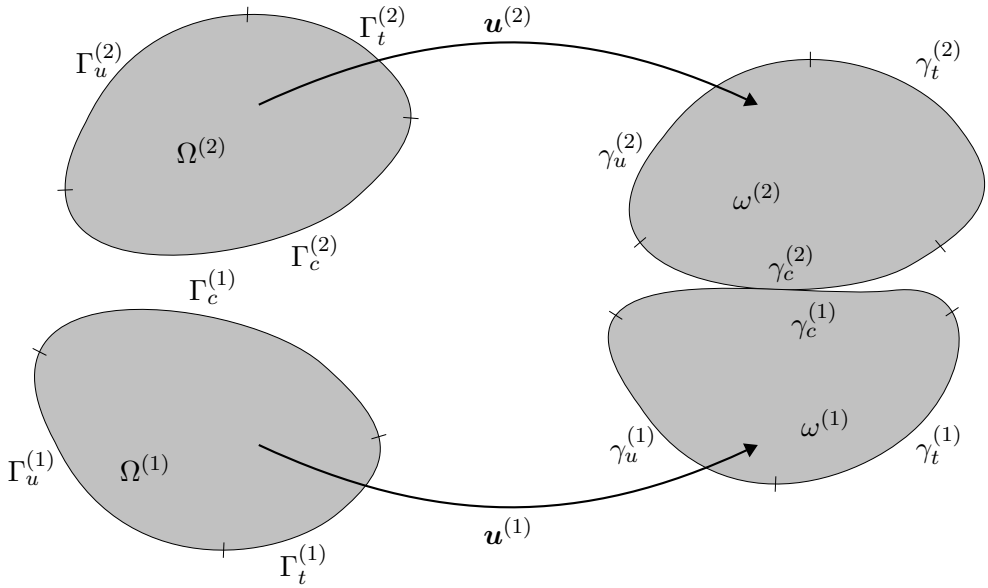

Figure 3.4: Continuum kinematics.

Equilibrium is then found from

$$\delta\Pi_{tot}(\boldsymbol{u}, \lambda, \delta\boldsymbol{u}, \delta\lambda) = \sum_{i=1}^{2} \delta\Pi(\boldsymbol{u}^{(i)}, \delta\boldsymbol{u}^{(i)}) + \delta\Pi_c(\boldsymbol{u}, \lambda, \delta\boldsymbol{u}, \delta\lambda) = 0, \qquad (3.13)$$

where

$$\delta\Pi_c(\boldsymbol{u}, \lambda, \delta\boldsymbol{u}, \delta\lambda) = \int_{\gamma_c} \delta\lambda g(\boldsymbol{u}) d\gamma + \int_{\gamma_c} \lambda\delta g(\boldsymbol{u}) d\gamma + \int_{\gamma_c} \lambda g(\boldsymbol{u}) \delta(d\gamma), \quad (3.14)$$

which should hold for all kinematically admissible $\delta\boldsymbol{u}$, that is $\delta\boldsymbol{u} = \boldsymbol{0}$ on Γ_u. In (3.14), the first term represents the weak non-penetration condition, the second term represents the virtual work of the contact pressure and the third term represents the complementary condition (3.8) in the weak sense. Since the complementary condition should be satisfied at the state of contact, this term is sometimes neglected (Puso and Laursen, 2004). As a consequence, the linearization of (3.13) becomes nonsymmetric, although the impact on the final result is typically negligible (Hiermeier et al., 2018).

3.4 Conventional contact methods

There are several methods to enforce the contact constraints and find equilibrium via (3.13). The subsequent section describes the most relevant methods.

3.4.1 Lagrange multiplier method

From an optimization perspective, Π_{tot} is a *Lagrangian* functional with Lagrange multiplier λ. In the *Lagrange multiplier method* (LMM), the saddle point problem in (3.13) is solved directly based on the contact potential energy

$$\Pi_c(\boldsymbol{u}, \lambda) = \int_{\gamma_c} \lambda g(\boldsymbol{u}) d\gamma, \tag{3.15}$$

where both $\boldsymbol{u}$ and λ are independent variables. The benefit of the LMM is that the contact constraints are enforced exactly. However, the discretization results in additional degrees of freedom for the Lagrange multiplier λ on the contact interface and an active set strategy has to be used to track active contact nodes. This is because the contact boundary is unknown before the solution is found, and an algorithm must keep track of where the contact is active throughout the solution procedure. The tangent matrix resulting from the linearization of the variation of (3.15) yields a system in which rows corresponding to inactive Lagrange multiplier degrees of freedom contain only zeros, rendering conventional solution methods such as Newton's method unsuitable. When using active set strategies the reduced system containing only the active Lagrange multiplier degrees of freedom can solved using so-called dual-shape functions where the discrete Lagrange multiplier degrees of freedom are eliminated via condensation (Wohlmuth, 2000; Hintermüller et al., 2002; Popp et al., 2009).

To summarize, the LMM provides an exact enforcement of the non-penetration constraint but is costly due to the additional degrees of freedom from the discretization of λ and due to the necessary active set strategy.

3.4.2 Penalty method

A straightforward method for modeling the contact interaction is the penalty method (PM), where the non-penetration constraint (3.5) is no longer strictly enforced. Instead, the contact pressure is modeled using

$$\lambda(\boldsymbol{u}) = \varepsilon \langle g(\boldsymbol{u}) \rangle_- = \varepsilon \min(g(\boldsymbol{u}), 0), \tag{3.16}$$

where ε is a user-defined *penalty parameter*. Thus, the contact potential energy becomes

$$\Pi_c(\boldsymbol{u}) = \int_{\gamma_c} \varepsilon \langle g(\boldsymbol{u}) \rangle_- g(\boldsymbol{u}) d\gamma. \tag{3.17}$$

This method relaxes the non-penetration constraint (3.5) by penalizing penetration between the contacting bodies, which is illustrated in Fig. 3.5. The PM automatically fulfills $\lambda(\boldsymbol{u}) \leq 0$ and requires no additional degrees of freedom for the contact pressure

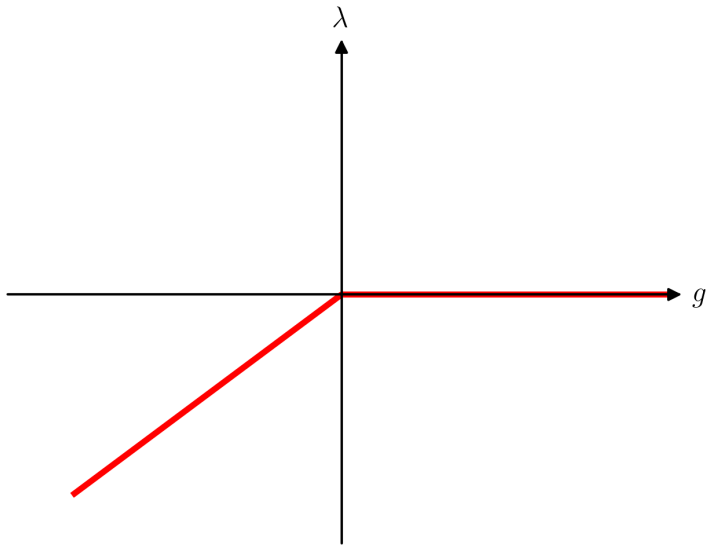

Figure 3.5: Contact pressure using the PM in (3.16).

which reduces the computational cost. From an implementation stand point the PM is appealing since integration can be performed over the entire potential contact surface γ_c without regard for active contact zones. By taking the variation of Π_c, the contact virtual work becomes

$$\delta\Pi_c(\boldsymbol{u}, \delta\boldsymbol{u}) = \int_{\gamma_c} \delta(\varepsilon\langle g(\boldsymbol{u})\rangle_{\text{-}})g(\boldsymbol{u}) + \varepsilon\langle g(\boldsymbol{u})\rangle_{\text{-}}\delta g(\boldsymbol{u})d\gamma + \int_{\gamma_c} \lambda g(\boldsymbol{u})\delta(d\gamma), \quad (3.18)$$

that is analogous to the virtual work of a traction on γ_c. The unconstrained system using the PM can be solved using e.g. Newton's method. By increasing the penalty parameter ε, the non-physical penetrations become smaller, but the resulting problem eventually becomes ill-conditioned. Consequently, the penalty parameter ε must be carefully chosen for each problem.

3.4.3 Augmented Lagrange method

A third alternative, that combines the ideas of the LMM and PM, is the Augmented Lagrange method (ALM) (Alart and Curnier, 1991). In this method, the Lagrange multiplier λ is replaced with the augmented multiplier $\hat{\lambda}$, which is commonly defined as

$$\hat{\lambda} = \langle \lambda + \varepsilon g(\boldsymbol{u})\rangle_{\text{-}}. \quad (3.19)$$

As opposed to the LMM there is no constraint on $\hat{\lambda}$. The result is an unconstrained problem where the potential contact energy is given by

$$\Pi_c(\boldsymbol{u}, \lambda) = \int_{\gamma_c} \hat{\lambda} g(\boldsymbol{u}) d\gamma. \tag{3.20}$$

Notably, using (3.20) yields a Lagrangian with the same solution as using (3.15) since the penalty contribution is zero when the contact constraints are exactly fulfilled. Instead of using an active set strategy (3.20) can be solved using the *Uzawa method* (Arrow et al., 1958) where first the displacement $\boldsymbol{u}^\star$ satisfying equilibrium for a fixed λ is found using e.g. Newton's method to solve

$$\begin{aligned} \boldsymbol{u}^\star &= \arg\min_{\boldsymbol{u}} \Big(\sum_{i=1}^{2} \Pi(\boldsymbol{u}^{(i)}) + \Pi_c(\boldsymbol{u}, \lambda)\Big), \\ \text{s.t.} \quad & \boldsymbol{u} = \bar{\boldsymbol{u}} \quad \text{on } \Gamma_u, \end{aligned} \tag{3.21}$$

and then the Lagrange multiplier is updated according to

$$\lambda \leftarrow< \lambda + \varepsilon g(\boldsymbol{u}^\star) >_-, \tag{3.22}$$

see Simo and Laursen (1992). This process is repeated until some user-defined criterion is reached, such as when the constraint violation becomes sufficiently small. The *Uzawa method* is illustrated in Fig. 3.6. Compared to the PM, the ALM using the *Uzawa method* can use a smaller penalization ε than the PM to achieve a satisfactory level of constraint violation. The benefit of using the Uzawa method with the ALM comes with the cost of requiring a nested solution method.

Alternatively, the contact potential energy can instead be defined as

$$\Pi_c(\boldsymbol{u}, \lambda) = \begin{cases} \int_{\gamma_c} (\lambda + \frac{\varepsilon}{2} g(\boldsymbol{u})) g(\boldsymbol{u}) d\gamma & \text{when } \lambda + \varepsilon g(\boldsymbol{u}) \leq 0, \\ \int_{\gamma_c} -\frac{\lambda^2}{2\varepsilon} d\gamma & \text{when } \lambda + \varepsilon g(\boldsymbol{u}) > 0, \end{cases} \tag{3.23}$$

and the resulting saddle-point problem can be solved for the Lagrange multiplier and the displacements simultaneously (Pietrzak and Curnier, 1999) although, like the LMM, the resulting system contains additional degrees of freedom for λ.

3.4.4 Barrier method

Similar to the PM, constraint enforcement can also be achieved using the barrier method (BM) that uses a barrier function

$$\lambda(\boldsymbol{u}) = -\frac{\mu}{g(\boldsymbol{u})}, \tag{3.24}$$

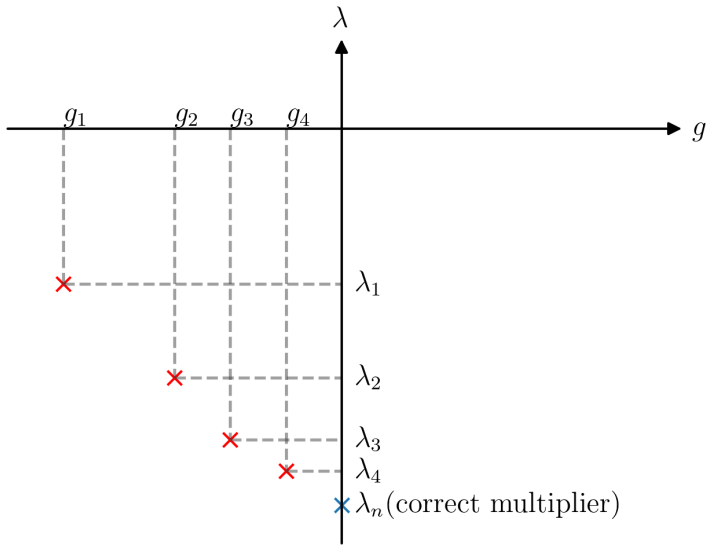

Figure 3.6: Illustration of the Uzawa scheme.

where μ is the barrier parameter (Wriggers and Laursen, 2006) and the contact potential energy becomes

$$\Pi_c(\boldsymbol{u}) = -\int_{\gamma_c} \frac{\mu}{g(\boldsymbol{u})} d\gamma. \tag{3.25}$$

No penetration is allowed with this method and the contact potential energy always contributes to the total energy Π_{tot}, although the contribution is small when the contacting bodies are distant. This behavior is illustrated in Fig. 3.7. As with penalty methods, the BM can result in an ill-conditioned problem when the barrier parameter μ becomes large. Furthermore, finding a starting point where all contacting bodies are sufficiently separated can also be a challenge.

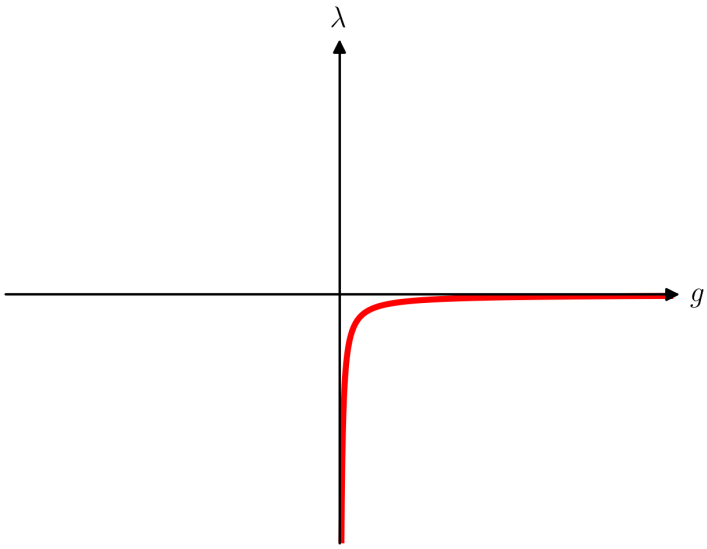

Figure 3.7: Contact pressure using the Barrier function (3.24).

3.5 The third medium contact method

As an alternative to directly modeling the contact between two bodies $\Omega^{(1)}$ and $\Omega^{(2)}$ using the contact constraints (3.9), a compliant medium $\Omega^{(m)}$ can be used to transfer contact forces. This provides a way to treat the contact constraints implicitly and is called the *third medium contact* method (TMC) (Wriggers et al., 2013). The TMC is similar to the BM in the sense that penetration is prevented by contact forces that are activated before the surfaces are in contact. An illustration of the TMC is provided in Fig. 3.8. Hyperelastic material models that fulfill the growth condition (2.12) are suit-

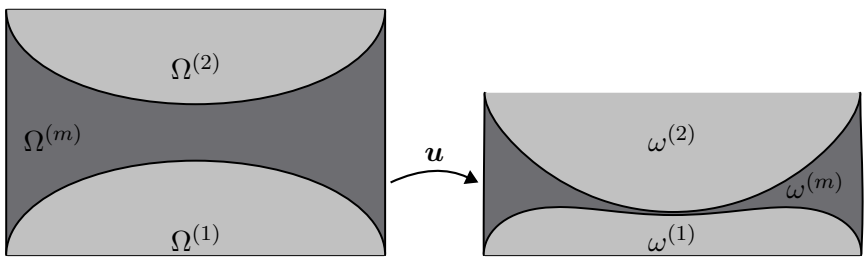

Figure 3.8: Third medium contact.

able for modeling the third medium and can be made highly compliant with suitable material parameters so that they do not give rise to significant contact forces before

contact occurs. A popular choice for the TMC is to use a compressible neo-Hookean material. Unfortunately, modeling the third medium with a conventional hyperelastic model is not sufficient for a stable contact model, since the third medium is prone to become highly distorted, which can cause trouble for numerical solvers. However, recent works (Bluhm et al., 2021; Faltus et al., 2024; Frederiksen et al., 2025; Wriggers et al., 2025) have developed regularization techniques that are able to stabilize the third medium by penalizing undesired deformation modes associated with the distortion such as bending or warping. An approach based on local changes of the rotation tensor $\boldsymbol{R}$ is proposed in paper E.

One choice for regularizing the third medium is to penalize the gradient of the deformation gradient (Bluhm et al., 2021). A suitable strain energy for the compliant medium $\Omega^{(m)}$ is then given by the compressible neo-Hookean energy W in (2.13), augmented with a regularization term, resulting in

$$W^{TM}(\boldsymbol{F}, \nabla \boldsymbol{F}) = W(\boldsymbol{F}) + \frac{k_r}{2} \nabla \boldsymbol{F} \vdots \nabla \boldsymbol{F}, \tag{3.26}$$

where $\vdots$ denotes the triple contraction and k_r is a penalization parameter. The regularized strain energy (3.26) penalizes several high-order deformation modes. This choice may be too strict causing the third medium to influence the solution outside contact. Furthermore, (3.26) also requires higher order elements. Regardless, (3.26) has proven useful for topology optimization and was used in Paper A for the design of metamaterials that utilize self-contact.

To illustrate the need for regularization in the third medium, consider the contact between two rectangular blocks that are pressed together, as shown in Fig. 3.9a. Clearly, the deformed grid without regularization in Fig. 3.9b becomes heavily distorted causing numerical solvers to fail with additional loading, whereas the regularized TMC stabilizes the numerical grid as shown in Fig. 3.9c.

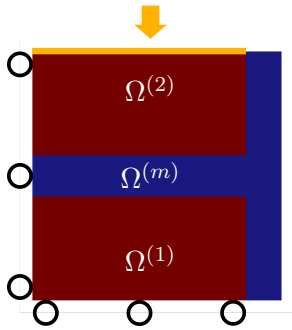

(a) Setup of TMC example.

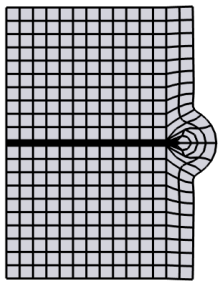

(b) Deformed grid without TMC regularization.

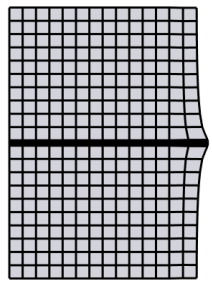

(c) Deformed grid with TMC regularization.

Figure 3.9: Contact between two blocks modeled using the third medium contact method.

Chapter 4

Numerical contact methods

In order to find the equilibrium given by (3.13), an accurate discretization of the contact interface γ_c is required. When discretized, the contacting surfaces become faceted and will in general not conform. The following chapter describes common methods to discretize γ_c and compute the contact virtual work $\delta\Pi_c(\boldsymbol{u}, \lambda)$.

4.1 Node-to-node discretization

A convenient way to discretize the contact constraints is to use the *node-to-node* (NTN) formulation. In this method, the contacting surfaces are discretized such that the coordinates of their nodes $\mathbf{x}_i^{(1)}$ and $\mathbf{x}_j^{(2)}$ match, as seen in Fig. 4.1. Consequently, the gap function in (3.4) can be computed for each node pair and the contact potential energy follows from

$$\Pi_c(\boldsymbol{u}, \lambda) = \int_{\gamma_c} \lambda g(\boldsymbol{u}) d\gamma \approx \sum_{i,j=1}^{n_{pairs}} A_i \lambda_i (\mathbf{x}_i^{(1)} - \mathbf{x}_j^{(2)}) \cdot \mathbf{n}^{(2)}, \tag{4.1}$$

where n_{pairs} is the number of nodal pairs, λ_i the nodal Lagrange multiplier and A_i is an area associated with each pair.

The strength of this formulation lies in its simplicity. The NTN can be leveraged when small deformations are considered and the grids match before and after deformation. On the other hand, since the contacting grids are required to match, sliding and large deformations are not allowed. As such, the NTN is suitable for structural optimization when the contact surface does not change.

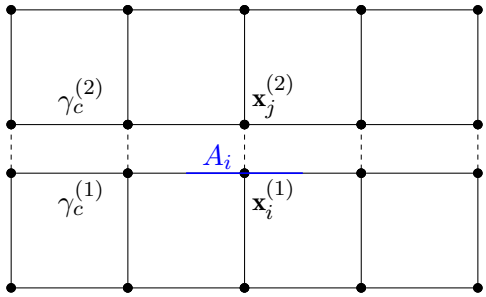

Figure 4.1: NTN discretization.

4.2 Node-to-segment

A widely used discretization method that is able to handle large deformations and finite sliding is the *node-to-segment* (NTS) method. In this method, the non-penetration condition (3.5) is enforced for the nodes on $\gamma_c^{(1)}$ (Wriggers and Laursen, 2006; Zavarise and De Lorenzis, 2009). Considering first-order elements, the contact potential work is computed over "contact elements" that consist of a node $\mathbf{x}_i^{(1)}$ on $\gamma_c^{(1)}$ and the line segment defined by the nodes $\mathbf{x}_j^{(2)}$ and $\mathbf{x}_k^{(2)}$ on $\gamma_c^{(2)}$, as illustrated in Fig. 4.2. The contribution to the contact potential, integrated on $\gamma_c^{(1)}$, is computed as

$$\begin{aligned}\Pi_c(\mathbf{u},\lambda) &= \sum_{i=1}^{n_c^{(1)}} \int_{\gamma_c^{(1)}} \lambda_i(\mathbf{x}_i^{(1)} - \mathbf{x}^{(2)}(\bar{\zeta})) \cdot \mathbf{n}^{(2)} d\gamma \\ &= \sum_{i=1}^{n_c^{(1)}} A_i \lambda_i(\mathbf{x}_i^{(1)} - \mathbf{x}^{(2)}(\bar{\zeta})) \cdot \mathbf{n}^{(2)}, \end{aligned} \tag{4.2}$$

where $n_c^{(1)}$ is the number of nodes on $\gamma_c^{(1)}$, A_i is the area associated with $\mathbf{x}_i^{(1)}$ and the position $\mathbf{x}^{(2)}(\bar{\zeta})$ is located between $\mathbf{x}_j^{(2)}$ and $\mathbf{x}_k^{(2)}$ and determined from the projection of $\mathbf{x}_i^{(1)}$ onto $\gamma^{(2)}$. The NTS discretization results in a collocation type method that enforces the contact constraints in the nodes of one of the contacting surfaces. The inherent bias of the NTS can be handled by so-called *two-pass* methods where (4.2) is computed once for each surface (Hallquist et al., 1985). Unfortunately, this approach can lead to locking as the problem becomes overconstrained (Kikuchi and Oden, 1988). Nevertheless, since the NTS method can handle non-matching grids it is a suitable for both shape and topology optimization, where evolving contact boundaries must be accommodated.

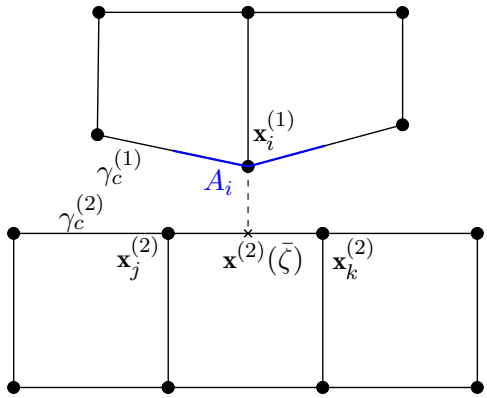

Figure 4.2: NTS discretization.

4.3 The mortar method

Instead of enforcing the contact constraints node-wise it is possible to enforce them weakly. Since contact surfaces become faceted after discretization, and the resulting grids are typically non-conforming, a point-wise enforcement of the non-penetration constraint can be undesirable. A weak constraint enforcement is leveraged in the *mortar method* where the potential contact energy is computed from

$$\Pi_c(\mathbf{u}, \lambda) \approx \int_{\gamma_c^{(1)}} \lambda(\xi^{(1)})(\mathbf{x}_i^{(1)}(\xi^{(1)}) - \mathbf{x}^{(2)}(\xi^{(2)}) \circ \chi) \cdot \mathbf{n} d\gamma, \tag{4.3}$$

where $\xi^{(1)}$ and $\xi^{(2)}$ are the finite element parameterizations and χ defines the mapping between $\gamma^{(1)}$ and $\gamma^{(2)}$ which depends on whether $\mathbf{n}^{(1)}$ or $\mathbf{n}^{(2)}$ is used. This is indicated by the omission of the superscript on $\mathbf{n}$. Compared to the NTN and NTS methods, the mortar formulation (4.3) integrates the contact contributions including the projection that finds $\xi^{(2)}$, over $\gamma_c^{(1)}$. Like the NTS, the mortar method is suitable for both shape and topology optimization.

4.3.1 Mortar discretization

The mortar discretization uses isoparametric finite elements and as such, the position $\boldsymbol{x}^{(i)}$ and virtual displacement $\delta\boldsymbol{u}^{(i)}$ are on each surface interpolated as

$$\boldsymbol{x}^{(i)} \approx \mathbf{x}^{(i)}(\xi^{(i)}) = \sum_{j=1}^{n_c^{(i)}} \phi_j^{(i)}(\xi^{(i)}) \mathbf{x}_j^{(i)}, \tag{4.4}$$

and

$$\delta \boldsymbol{u}^{(i)} \approx \delta \mathbf{u}^{(i)}(\xi^{(i)}) = \sum_{j=1}^{n_c^{(i)}} \phi_j^{(i)}(\xi^{(i)}) \delta \mathbf{a}_j^{(i)}, \tag{4.5}$$

where $\phi^{(i)}$ are the finite element basis functions and $n_c^{(i)}$ are the number of nodes on the contact surfaces $\gamma_c^{(i)}$. A common choice in mortar methods is to use $\gamma_c = \gamma_c^{(1)}$ wherefore it makes sense to also interpolate the Lagrange multiplier λ on $\gamma_c^{(1)}$ via

$$\lambda \approx \lambda(\xi^{(1)}) = \sum_{j=1}^{n_c^{(1)}} \phi_j^{(1)}(\xi^{(1)}) \lambda_j. \tag{4.6}$$

4.3.2 Evaluation of the mortar integrals

Two mortar-type methods are used herein to compute the integral in (4.3). In paper B, *element-based* integration is used, while in papers C and D *segment-based* integration is used. A comparison of these methods can be found in Farah et al. (2015).

4.3.3 Element-based integration

The element-based integration is based on the gap function (3.4) and uses Gaussian quadrature on the boundaries of the potential contact elements e on $\gamma^{(1)}$ (Fischer and Wriggers, 2005; Wriggers and Laursen, 2006). For every integration point $\xi_p^{(1)}$, a corresponding point $\boldsymbol{x}^{(2)}(\xi^{(2)}(\xi_p^{(1)}))$ is found through the closest point projection. Consider two opposing first-order segments on the elements $e^{(1)}$ and $e^{(2)}$ with element nodes $(\mathbf{x}_1^{(1)}, \mathbf{x}_2^{(1)})$ and $(\mathbf{x}_1^{(2)}, \mathbf{x}_2^{(2)})$, respectively. Assuming that (3.1) is convex, the solution of (3.2) becomes

$$\bar{\zeta}_p = \xi^{(2)}(\xi_p^{(1)}) = \frac{1}{||\mathbf{x}_2^{(2)} - \mathbf{x}_1^{(2)}||_2^2} (\mathbf{x}^{(1)}(\xi_p^{(1)}) - \mathbf{x}_1^{(2)}) \cdot (\mathbf{x}_2^{(2)} - \mathbf{x}_1^{(2)}), \tag{4.7}$$

as illustrated in Fig. 4.3. The discretized virtual work contribution follows from

$$\Pi_c^{el}(\mathbf{u}, \lambda) = \sum_{p=1}^{n_p} \pi_{c,p}^{el}(\mathbf{u}, \lambda) w_p \mathrm{J}_p, \tag{4.8}$$

where

$$\pi_{c,p}^{el}(\mathbf{u}, \lambda) = \sum_{i=1}^{n_c^{(1)}} \phi_i^{(1)}(\xi_p^{(1)}) \lambda_i \Big(\sum_{j=1}^{n_c^{(1)}} \phi_j^{(1)}(\xi_p^{(1)}) \mathbf{x}_j^{(1)} - \sum_{k=1}^{n_c^{(2)}} \phi_k^{(2)}(\bar{\zeta}_p) \mathbf{x}_k^{(2)} \Big) \cdot \mathbf{n}^{(2)}. \tag{4.9}$$

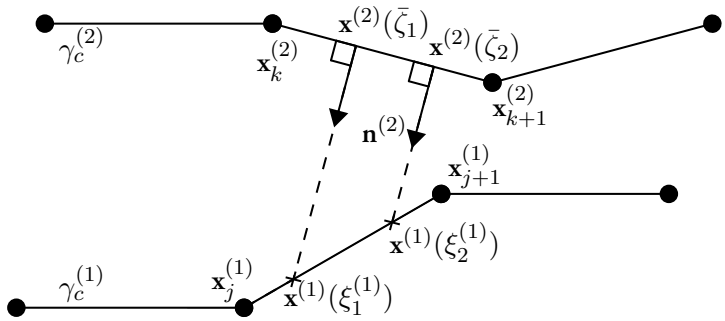

Figure 4.3: Gauss point projection used in the element-based integration for $n_p = 2$.

In (4.9), $\mathbf{n}^{(2)}$ is the normal to the element to which $\bar{\zeta}_p$ belongs, n_p denotes the number of integration points with corresponding weights w_p and J_p is the Jacobian of the mapping from the element with nodal coordinates $\mathbf{x}_1^{(1)}$ and $\mathbf{x}_2^{(1)}$ to the isoparametric domain.

The element based mortar method is used in paper B to tailor the force-displacement response of hyperelastic structures.

4.3.4 Segment-based integration

The segment-based integration employs a continuous normal field, which enables the definition of a gap function that remains continuous across element boundaries, as opposed to the element-based integration which relies on projections using the element-wise constant normals $\mathbf{n}^{(2)}$. To construct the continuous normal field, use is made of weighted average nodal normals $\bar{\mathbf{n}}_j^{(1)}$. For the node j shared by two adjacent segments $e^{(1)}$ and $e^{(2)}$ with normals $\boldsymbol{n}_{e1}$ and $\boldsymbol{n}_{e2}$ and corresponding lengths l_{e1} and l_{e2}, the weighted average nodal normal $\bar{\mathbf{n}}_j^{(1)}$ is given by

$$\bar{\mathbf{n}}_j^{(1)} = \frac{l_{e2}\mathbf{n}_{e1}^{(1)} + l_{e1}\mathbf{n}_{e2}^{(1)}}{||l_{e2}\mathbf{n}_{e1}^{(1)} + l_{e1}\mathbf{n}_{e2}^{(1)}||_2}. \tag{4.10}$$

The continuous normal field is constructed from

$$\tilde{\mathbf{n}}^{(1)}(\xi^{(1)}) = \sum_{i=1}^{n_e} \phi_i^{(1)}(\xi^{(1)})\bar{\mathbf{n}}_i^{(1)}, \tag{4.11}$$

where n_e is the number of nodes on element face e where $\tilde{\mathbf{n}}^{(1)}(\xi^{(1)})$ is evaluated. The contact segments on which the mortar integrals are evaluated are constructed based on (4.11) and the endpoints of each segment are defined by:

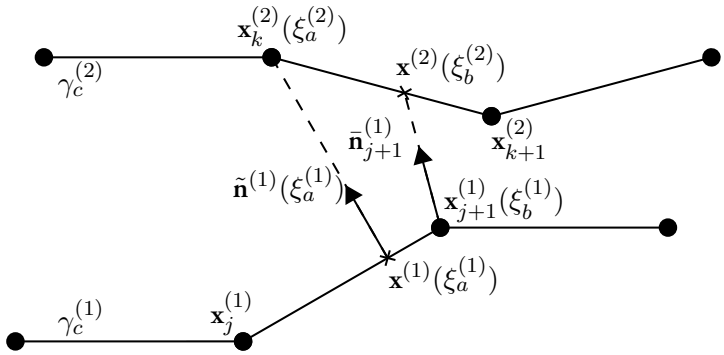

Figure 4.4: Construction of contact segments based on the continuous normal $\tilde{\mathbf{n}}^{(1)}$.

- the coordinate $\mathbf{x}^{(1)}(\xi_a^{(1)})$ from which the line in the direction of $\tilde{\mathbf{n}}^{(1)}(\xi_a^{(1)})$ intersects the nodal coordinate $\mathbf{x}_k^{(2)}(\xi_a^{(2)})$,
- the nodal coordinate $\mathbf{x}_{j+1}^{(1)}(\xi_b^{(1)})$ and its projection onto $\gamma_c^{(2)}$, $\mathbf{x}^{(2)}(\xi_b^{(2)})$, along $\bar{\mathbf{n}}_{j+1}$,

as illustrated in Fig. 4.4. The endpoint $\mathbf{x}^{(1)}(\xi_a^{(1)})$ is found by solving

$$\left[\mathbf{x}^{(1)}(\xi_a^{(1)}) - \mathbf{x}_k^{(2)}\right] \times \tilde{\mathbf{n}}^{(1)}(\xi_a^{(1)}) = \mathbf{0}. \tag{4.12}$$

To find the other segment endpoint $\mathbf{x}^2(\xi_b^2)$ associated with the first projection, the following equation is solved

$$\left[\mathbf{x}^{(2)}(\xi_b^2) - \mathbf{x}_{j+1}^{(1)}\right] \times \bar{\mathbf{n}}_{j+1}^{(1)} = \mathbf{0}. \tag{4.13}$$

Having the projected points $\xi_a^{(1)}$ and $\xi_b^{(2)}$ the contact segment is parameterized as

$$\xi^{(i)}(\varphi) = \frac{1}{2}(1-\varphi)\xi_a^{(i)} + \frac{1}{2}(1+\varphi)\xi_b^{(i)}. \tag{4.14}$$

Denoting the quadrature points $\xi_p^{(i)} = \xi^{(i)}(\varphi_p)$, the contact virtual work contribution in each segment follows from

$$\Pi_c^{seg}(\mathbf{u},\lambda) = \sum_{p=1}^{n_p} \pi_{c,p}^{seg}(\mathbf{u},\lambda) w_p J_{seg}, \tag{4.15}$$

where

$$\pi_{c,p}^{seg}(\mathbf{u},\lambda) = \sum_{i=1}^{n_c^{(1)}} \phi_i^{(1)}(\xi_p^{(1)})\lambda_i \bar{\mathbf{n}}_i^{(1)} \cdot \Big(\sum_{j=1}^{n_c^{(1)}} \phi_j^{(1)}(\xi_p^{(1)})\mathbf{x}_j^{(1)} - \sum_{k=1}^{n_c^{(2)}} \phi_k^{(2)}(\xi_p^{(2)})\mathbf{x}_k^{(2)}\Big), \tag{4.16}$$

J_{seg} is the Jacobian of the mapping from the global coordinate system to the parameterized segment and $n_c^{(i)}$ is the number of nodes on each contact surface.

The segment-based mortar method is used in paper C where a shape optimization regularization that accounts for the contact constraints is developed and applied to several examples. This method is extended to include topology optimization in paper D.

Chapter 5

Structural optimization

Structural optimization aims to find the best performing structure with regards to the objective $g_0(x)$, and a set of constraints $g_i(x) \leq 0$, in terms of the design variables x that describe the design. The widely used topology optimization (TO), will for instance optimize the entire material layout within a given design domain, commonly using a density field or a level set contour. If the optimization is restricted to the structural boundaries of the design the method is instead called shape optimization (SO). The structural optimization problem can be stated as

$$\min_x \; g_0(x), \tag{5.1}$$

$$\text{s.t } g_i(x) \leq 0 \quad i = 1, 2, \ldots, m, \tag{5.2}$$

$$x_l \leq x \leq x_u, \tag{5.3}$$

where $[x_l, x_u]$ are box constraints on x and m are the number of constraints.

5.1 Shape optimization

In order to formulate a structural SO problem, the objective g_0 and constraint functions g_i need to be parameterized. A straightforward approach is to parameterize the geometry using the finite element mesh with nodes $\mathbf{X}_k$. While tempting due to its simplicity, this strategy is prone to several numerical difficulties such as jagged boundaries and inverted elements (Braibant and Fleury, 1984; Haftka and Grandhi, 1986).

5.1.1 Spline parameterization

One way to alleviate the issues associated with the direct optimization of the nodal coordinates is to parameterize the shape using splines. By construction, continuity

in the geometry of the design can be incorporated via the spline representation. A popular choice is to use B-splines (Braibant and Fleury, 1984), that can be considered a special case of so-called NURBS (non-uniform rational B-spline), which are widely used in computer aided design (CAD) systems.

A B-spline curve $\mathbf{X}(u, \mathbf{V}_i)$ of degree p, parameterized by u is formed from the linear combination of the piecewise defined B-spline basis functions $B_{i,p}(u)$ and the control points $\mathbf{V}_i$ according to

$$\mathbf{X}(u, \mathbf{V}_i) = \sum_{i=1}^{n} B_{i,p}(u)\mathbf{V}_i. \tag{5.4}$$

The B-spline basis functions are defined recursively on intervals based on the knot vector U of non-decreasing values $U = [u_0, u_1, \ldots, u_{p+n+1}]$ (De Boor, 1972), starting at $p = 0$ with

$$B_{i,0}(u) = \begin{cases} 1 \text{ if } u_i \leq u < u_{i+1}, \\ 0 \text{ otherwise,} \end{cases} \tag{5.5}$$

and the higher order basis functions follow from

$$B_{i,p}(u) = \frac{u - u_i}{u_{i+p} - u_i} B_{i,p-1}(u) + \frac{u_{i+p+1} - u}{u_{i+p+1} - u_{i+1}} B_{i+1,p-1}(u). \tag{5.6}$$

Fig. 5.1 illustrates B-spline basis functions up to order $p = 2$, where, by repeating the first and last knots the spline becomes clamped. Clamping of B-splines is necessary when the spline should pass through the first and last control points. This is because B-splines are C^{p-r_j} continuous in each knot u_j, where the multiplicity r_j is the number of times the knot value u_j is repeated. To use B-splines in SO, a surface $\mathbf{S}(u, v, \mathbf{V}_{i,j})$ can be constructed by forming the dyad of two B-splines, i.e.

$$\mathbf{S}(u, v, \mathbf{V}_{i,j}) = \sum_{i=0}^{n} \sum_{j=0}^{m} B_{i,p}(u) B_{j,q}(v) \mathbf{V}_{i,j}, \tag{5.7}$$

where $\mathbf{V}_{i,j}$ are the control points and $m + 1$ is the number of control points for the second B-spline curve of order q. Upon evaluating $\mathbf{S}(u, v, \mathbf{V}_{i,j})$ for a set of points (u_k, v_k) it is possible to construct a finite element grid, as illustrated in Fig. 5.2. The grid generated from the B-spline surface can be used to compute the structural performance. Using B-splines provides smoothness to the SO which helps circumvent problems due to jagged and inverted grids. It is possible to choose either the control points $\mathbf{V}_{i,j}$, the knots (u_i, v_j) or both as design variables for SO. B-splines are used in paper A to SO contacting structures to tailor their force-displacement response.

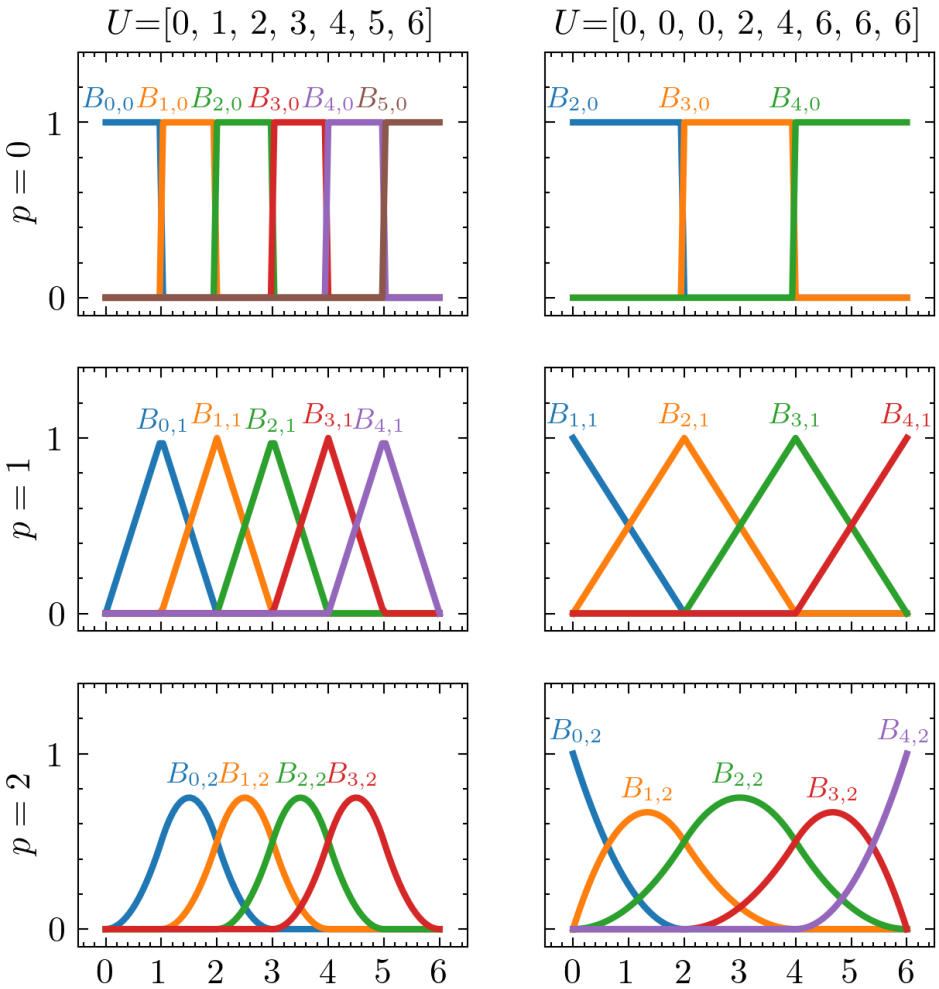

Figure 5.1: B-spline basis functions using two different knot vectors.

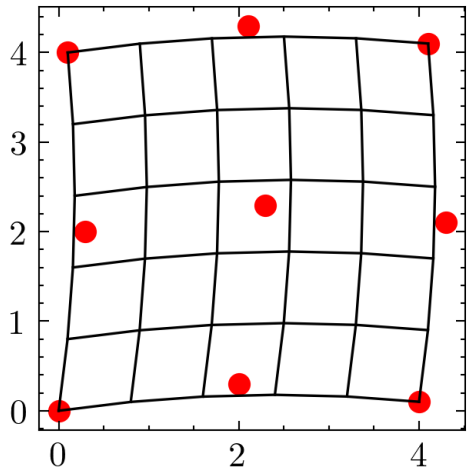

Figure 5.2: Grid generated from the dyad of two second order B-splines with knot vectors $U = V = [0, 0, 0, 6, 6, 6]$ and control points marked in red.

5.1.2 Filtering

The numerical issues associated with node-based SO can also be avoided using schemes that filter the shape change. In this case, the structural performance is computed based on the filtered shape with points $\mathbf{X}$. For the research in this thesis, $\mathbf{X}$ is obtained as the solution to a partial differential equation akin to the elastic state problem (2.8). The properties of this PDE can be chosen to control the SO in such a way that severe distortions of the design mesh are avoided in the optimization. The approach is inspired by Scherer et al. (2010); Swartz et al. (2023); Dahlberg et al. (2025), wherein the shape change $\mathbf{\Psi}$ takes points $\mathbf{X}_0$ in the "unoptimized" domain Ω_0 to the reference domain Ω with coordinates $\mathbf{X} = \mathbf{X}_0 + \mathbf{\Psi}$. The shape change $\mathbf{\Psi}$ is controlled by minimization of the potential $\tilde{\Pi}$ via

$$\min_{\mathbf{\Psi}} \tilde{\Pi}(\mathbf{\Psi}) = \min_{\mathbf{\Psi}} \int_{\Omega_0} \tilde{W}(\mathbf{\Psi}) d\Omega + \frac{k_d}{2} \int_{\Gamma_{0,d}} ||\mathbf{\Psi} - \mathbf{d}||_2^2 d\Gamma_0, \qquad (5.8)$$
$$\text{s.t. } \tilde{\mathbf{\Psi}} = \mathbf{0} \text{ on } \Gamma_{0,\Psi},$$

where $\tilde{W}$ is a *fictitious* hyperelastic strain energy function, k_d is a penalization parameter and $\mathbf{d}$ are the design variables that are defined on the boundary $\Gamma_{0,d}$ of Ω_0. The SO regularization (5.8) can be interpreted as a fictitious equilibrium problem where a bed of fictitious springs with "stiffness" k_d are attached to $\Gamma_{0,d}$ at one end, and pulled a distance $\mathbf{d}$ at the other, as illustrated in Fig 5.3. By tuning the properties of $\tilde{W}(\mathbf{\Psi})$ the characteristics of the shape change $\mathbf{\Psi}$ can be controlled. Specifically, the fictitious

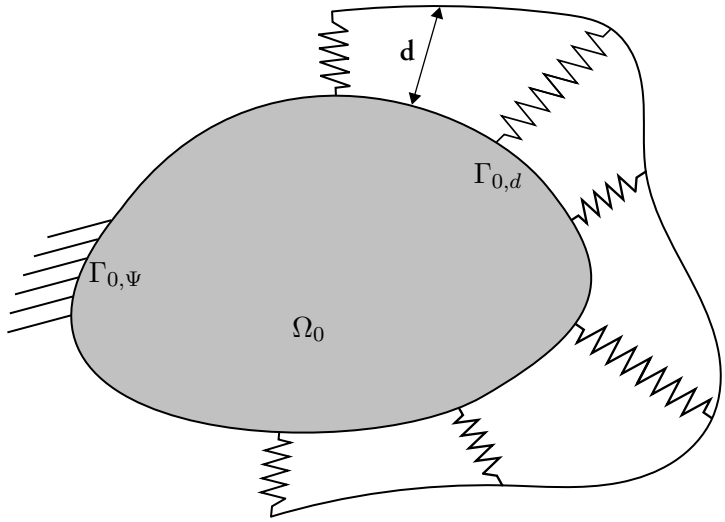

Figure 5.3: Illustration of the PDE based SO regularization.

strain energy $\tilde{W}(\boldsymbol{\Psi})$ is in this thesis modeled using a compressible neo-Hookean formulation (2.13), wherefore the fictitious bulk and shear moduli can be tuned to yield a high resistance to dilatational shape changes to avoid distorted elements.

SO using (5.8) is illustrated in Fig. 5.4 where a plate with a rectangular hole subject to a biaxial load is optimized for increased stiffness under a volume constraint, using node-based SO. As seen in Fig. 5.4b, without regularization, elements on the inner boundary become inverted which subsequently causes the optimization to stop. This is avoided when using regularization, as illustrated in Fig. 5.4c. Evidently, the formulation provides a straightforward formulation that requires no additional parameterization. The approach using (5.8) is used in papers A, C and D.

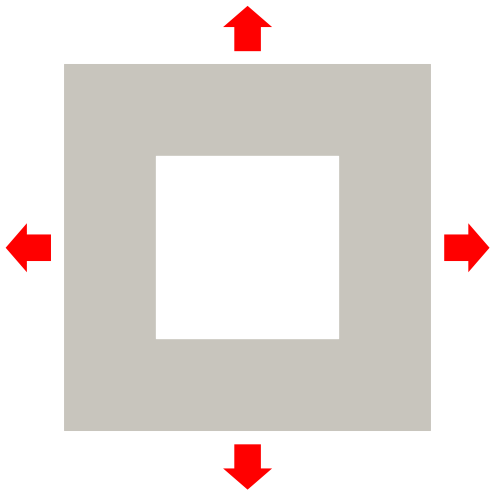

(a) Biaxially loaded plate with a rectangular hole.

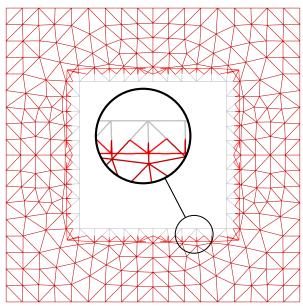

(b) Reference grid (gray) and shape optimized grid (red) using node based SO without regularization.

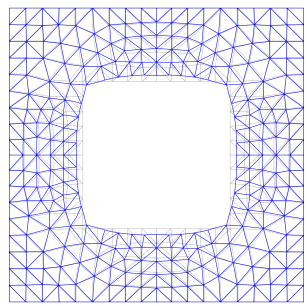

(c) Reference grid (gray) and shape optimized grid (blue) using node based SO with regularization.

Figure 5.4: Illustration of node-based SO with and without regularization.

5.2 Density-based topology optimization

In contrast to SO, TO is able to nucleate and remove holes in the design, providing an overall larger design freedom compared to SO. Density-based topology optimization uses a *density-field* $z \in [0, 1]$, where $z = 0$ corresponds to void and $z = 1$ corresponds to solid material. Typically, the density is used to scale the Young's modulus, so the objective and constraints can be formulated in terms of the density field, as $g_0 = g_0(\boldsymbol{u}(z), z)$ and $g_i = g_i(\boldsymbol{u}(z), z)$. While the ideal is to use binary values for z, the resulting integer optimization problem is not suitable for gradient based optimization algorithms. Instead, z is defined as a continuous variable for which the gradients are readily available. However, the solution to the resulting optimization problem can utilize intermediate densities $0 \leq z \leq 1$, which is undesirable as there is no clear interpretation of the design outside of plane conditions where z can be interpreted as the out-of-plane thickness. Thus, to make intermediate densities unfavorable in the optimization, it is common to introduce a penalization function. Two common penalization functions are the SIMP (Solid Isotropic Material with Penalization) and RAMP (Rational Approximation of Material Properties) schemes. In the SIMP approach, the Young's modulus E is given by

$$E(z) = \delta_0 + (1 - \delta_0) z^{q_s} E_0, \tag{5.9}$$

where δ_0 is the small residual value that prevents E from vanishing, E_0 is the Young's modulus of solid material and q_s is the penalization parameter (Bendsøe, 1989; Sigmund and Torquato, 1997). Alternatively, in the RAMP scheme the Young's modulus is given by

$$E(z) = \left(\delta_0 + \frac{z(1 - \delta_0)}{1 + q_r(1 - z)} \right) E_0, \tag{5.10}$$

where q_r is a penalization parameter. Notably, (5.10) has a non-vanishing sensitivity for $z = 0$ (Stolpe and Svanberg, 2001). The SIMP and RAMP schemes are illustrated in Fig. 5.5a and Fig. 5.5b, respectively. It can be seen that for increasing values of the penalization parameters q_s and q_r, the SIMP and RAMP schemes drive the Young's modulus of intermediate densities towards δ_0 or E_0. Consequently, when stiffness is maximized under a volume constraint, a $0 - 1$ design is favorable.

Due to the penalization of z, the TO problem becomes mesh dependent. In order to remove this dependency and regularize the TO, a length scale can be introduced via a filter that yields a smooth field ρ based on z. Herein, the so-called PDE-filter (Lazarov and Sigmund, 2011) is used. The PDE-filter is based a diffusion-type equation that filters z via minimization of the potential

$$\Pi_\rho(\rho) = \frac{1}{2} \int_\Omega l_0^2 |\nabla \rho|^2 d\Omega + \frac{1}{2} \int_\Omega (\rho - z)^2 d\Omega, \tag{5.11}$$

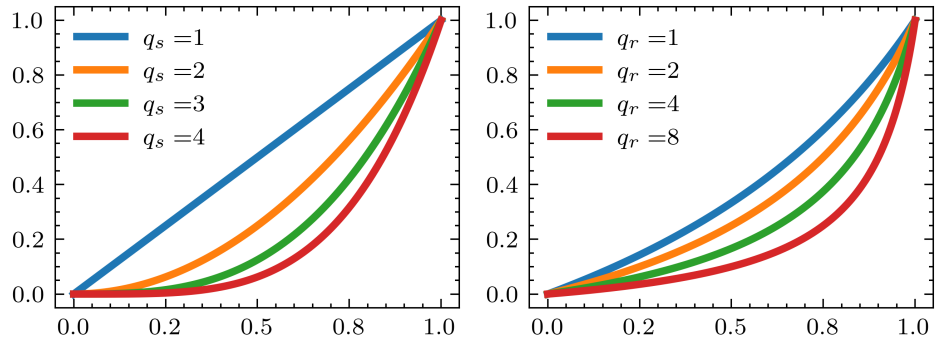

(a) SIMP interpolation for various values of q_s.

(b) RAMP interpolation for various values of q_r.

with respect to ρ, subject to $\nabla\rho \cdot \boldsymbol{N} = 0$ along the boundary $\partial\Omega$ of Ω. In (5.11), l_0 is the filter length scale parameter and $\delta\rho$ is the arbitrary virtual variation of ρ. The regularization (5.11) forces $||\rho - z||$ to be small, i.e. ρ to be similar to z while also placing a cost on large gradients $\nabla\rho$ to minimize oscillation in the field.

The filter (5.11) provides a smooth density field with an intrinsic length scale, but it will also "smear" the density field such that the transition from solid to void will contain regions with intermediate densities. In turn, the boundary definition is not unique. To make the transition from solid to void sharper a threshold projection is frequently used. In the limit, this can be realized using the Heaviside step function H with threshold η. However, this makes the problem non-differentiable at η, and instead, an approximate Heaviside projection is utilized, where the projected density $\tilde{\rho}$ is found from

$$\tilde{\rho}(\rho) = \frac{\tanh(\beta\eta) + \tanh(\beta(\rho - \eta))}{\tanh(\beta\eta) + \tanh(\beta(1 - \eta))}. \tag{5.12}$$

In (5.12) β controls the steepness of the approximate Heaviside function, as illustrated in Fig. 5.6. The effect of (5.12) is illustrated in Fig. 5.7.

TO is used in papers A and D. In paper A, the third medium contact method is used to model self-contact in metamaterials, whereby the void material $\rho \approx 0$ is used to transfer contact forces. In paper D, the mortar method is used instead to model contact between structures that are designed using both TO and SO.

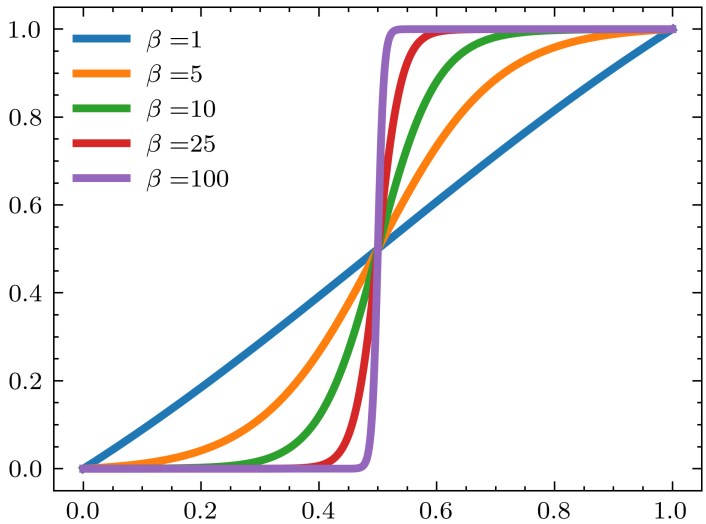

Figure 5.6: Approximate Heaviside projection for $\eta = 0.5$ and varying values of β.

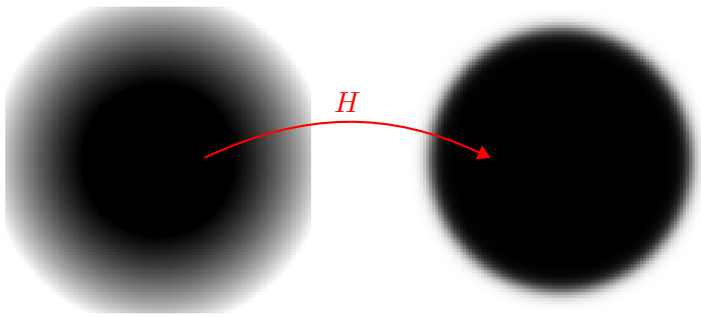

Figure 5.7: Approximate Heaviside projection applied to a grayscale image.

Chapter 6

Future work

The present work has developed methods for the structural optimization of deformable structures in frictionless contact, which can be beneficial in many engineering applications by enabling the design of structures that better exploit contact interactions. However, several areas of engineering utilize not only normal contact but also friction. Frictional contact is an important and challenging topic in contact mechanics, that has been outside the scope of this research. Modeling friction requires accurate and reliable models of the normal contact, so the work herein is a stepping stone for future research in this area. The main difficulty of including friction is to accommodate the path dependence associated with frictional sliding, which not only makes the sensitivity analysis more tedious but the additional non-smoothness also presents a challenge for optimization algorithms. Naturally, the study of friction enables the study of topics in tribology such as lubrication and wear.

Future research could also focus on extending the mortar-based methodologies developed in this thesis to three-dimensional formulations, enabling the study of more realistic and industrially relevant engineering applications.

Moreover, as demonstrated in Papers A and E, the TMC method has strong potential for accurate and robust contact modeling, particularly within topology optimization. Important avenues for future work include incorporating frictional contact and applying the methodology from Paper E to structural optimization problems.

Chapter 7

Summary of the appended papers

Paper A: Inverse homogenization is used to design metamaterials that exploit internal contact to achieve desired macroscopic stress-strain behavior. The metamaterials are designed using topology optimization followed by shape optimization and the third medium contact method is used to model the internal contact. A post-processing analysis using conventional contact algorithms is performed.

Paper B: Shape optimization is used to tailor the mechanical response of hyperelastic structures in frictionless contact. B-splines are used to parameterize the shape of the designs and the contact is modeled using the mortar method, which accommodates non-matching grids. The formulation is used to design axisymmetric structures that exhibit a near constant force in a given displacement interval which is useful for protective structures.

Paper C: A method for shape optimization of structures in frictionless contact that avoids excessive interference caused by design changes via a novel regularization is developed. In traditional shape optimization, the structures are "unaware" of each other outside of contact so that shape updates can result in significant interference between the structures. The proposed regularization controls the interference caused by shape changes which prevents the optimization scheme from exploiting interference that could cause the state problem to diverge. Contact is modeled using the mortar method and the numerical examples illustrate how the regularization can be used to optimize the contact response.

Paper D: Shape optimization using the contact aware formulation in Paper C is combined with density-based topology optimization to design contacting structures. The proposed formulation combines the design freedom of topology optimization with the ability of the shape optimization formulations to alter the shape of the contact boundaries. Sequential and simultaneous topology and shape optimization strategies are compared.

Paper E: A novel regularization for the third medium contact method is developed. Previously, the third medium contact method has been regularized through penalization of first- and second-order deformation modes. The proposed regularization is based on local changes of the rotation tensor instead, which avoids penalization of higher order deformation modes and can be used with first order elements.

Bibliography

Alart, P., Curnier, A., 1991. A mixed formulation for frictional contact problems prone to newton like solution methods. Computer methods in applied mechanics and engineering 92, 353–375.

Allaire, G., Jouve, F., Toader, A.M., 2002. A level-set method for shape optimization. Comptes rendus. Mathématique 334, 1125–1130.

Arrow, K.J., Hurwicz, L., Uzawa, H., Chenery, H.B., Johnson, S., Karlin, S., 1958. Studies in linear and non-linear programming. volume 2. Stanford University Press Stanford.

Azegami, H., Wu, Z.C., 1996. Domain optimization analysis in linear elastic problems: approach using traction method. JSME international journal. Ser. A, Mechanics and material engineering 39, 272–278.

Bendsøe, M.P., 1989. Optimal shape design as a material distribution problem. Structural Optimization 1, 193–202.

Bendsøe, M.P., Kikuchi, N., 1988. Generating optimal topologies in structural design using a homogenization method. Computer Methods in Applied Mechanics and Engineering 71, 197–224.

Beremlijski, P., Haslinger, J., Kocvara, M., Outrata, J., 2002. Shape optimization in contact problems with coulomb friction. SIAM Journal on Optimization 13, 561–587.

Bletzinger, K.U., Maute, K., 1997. Towards generalized shape and topology optimization. Engineering Optimization 29, 201–216.

Bluhm, G.L., Sigmund, O., Poulios, K., 2021. Internal contact modeling for finite strain topology optimization. Computational Mechanics 67, 1099–1114.

Borrvall, T., Petersson, J., 2001. Large-scale topology optimization in 3d using parallel

computing. Computer methods in applied mechanics and engineering 190, 6201–6229.

Braibant, V., Fleury, C., 1984. Shape optimal design using b-splines. Computer Methods in Applied Mechanics and Engineering 44, 247–267.

Bruggi, M., Duysinx, P., 2013. A stress–based approach to the optimal design of structures with unilateral behavior of material or supports. Structural and Multidisciplinary Optimization 48, 311–326.

Dahlberg, V., Dalklint, A., Wallin, M., 2025. Simultaneous shape and topology optimization on unstructured grids. Computer Methods in Applied Mechanics and Engineering 438, 117830.

Dalklint, A., Alexandersen, J., Frederiksen, A.H., Poulios, K., Sigmund, O., 2025. Topology optimization of contact-aided thermo-mechanical regulators. International Journal for Numerical Methods in Engineering 126, e7661.

Dalklint, A., Sjövall, F., Wallin, M., Watts, S., Tortorelli, D., 2023. Computational design of metamaterials with self contact. Computer Methods in Applied Mechanics and Engineering 417, 116424.

Dbouk, T., 2017. A review about the engineering design of optimal heat transfer systems using topology optimization. Applied Thermal Engineering 112, 841–854.

De Boor, C., 1972. On calculating with b-splines. Journal of Approximation theory 6, 50–62.

Duysinx, P., Bendsøe, M.P., 1998. Topology optimization of continuum structures with local stress constraints. International journal for numerical methods in engineering 43, 1453–1478.

Duysinx, P., Van Miegroet, L., Jacobs, T., Fleury, C., 2006. Generalized shape optimization using x-fem and level set methods, in: IUTAM symposium on topological design optimization of structures, machines and materials: status and perspectives, Springer. pp. 23–32.

Faltus, O., Horák, M., Doškář, M., Rokoš, O., 2024. Third medium finite element contact formulation for pneumatically actuated systems. Computer Methods in Applied Mechanics and Engineering 431, 117262.

Fancello, E., 2006. Topology optimization for minimum mass design considering local failure constraints and contact boundary conditions. Structural and Multidisciplinary Optimization 32, 229–240.

Farah, P., Popp, A., Wall, W.A., 2015. Segment-based vs. element-based integration for mortar methods in computational contact mechanics. Computational Mechanics 55, 209–228.

Fernandez, F., Puso, M.A., Solberg, J., Tortorelli, D.A., 2020. Topology optimization of multiple deformable bodies in contact with large deformations. Computer Methods in Applied Mechanics and Engineering 371, 113288.

Fischer, K., Wriggers, P., 2005. Frictionless 2d contact formulations for finite deformations based on the mortar method. Computational Mechanics 36, 226–244.

Frederiksen, A.H., Dalklint, A., Sigmund, O., Poulios, K., 2025. Improved third medium formulation for 3d topology optimization with contact. Computer Methods in Applied Mechanics and Engineering 436, 117595.

Frederiksen, A.H., Sigmund, O., Poulios, K., 2024. Topology optimization of self-contacting structures. Computational Mechanics 73, 967–981.

Gersborg-Hansen, A., Bendsøe, M.P., Sigmund, O., 2006. Topology optimization of heat conduction problems using the finite volume method. Structural and multidisciplinary optimization 31, 251–259.

Haftka, R.T., Grandhi, R.V., 1986. Structural shape optimization—a survey. Computer Methods in Applied Mechanics and Engineering 57, 91–106.

Hallquist, J., Goudreau, G., Benson, D., 1985. Sliding interfaces with contact-impact in large-scale lagrangian computations. Computer methods in applied mechanics and engineering 51, 107–137.

Hiermeier, M., Wall, W.A., Popp, A., 2018. A truly variationally consistent and symmetric mortar-based contact formulation for finite deformation solid mechanics. Computer Methods in Applied Mechanics and Engineering 342, 532–560.

Hilding, D., Torstenfelt, B., Klarbring, A., 2001. A computational methodology for shape optimization of structures in frictionless contact. Computer methods in applied mechanics and engineering 190, 4043–4060.

Hintermüller, M., Ito, K., Kunisch, K., 2002. The primal-dual active set strategy as a semismooth newton method. SIAM Journal on Optimization 13, 865–888.

Hojjat, M., Stavropoulou, E., Bletzinger, K.U., 2014. The vertex morphing method for node-based shape optimization. Computer Methods in Applied Mechanics and Engineering 268, 494–513.

Holmberg, E., Torstenfelt, B., Klarbring, A., 2013. Stress constrained topology optimization. Structural and Multidisciplinary Optimization 48, 33–47.

Holzapfel, G.A., 2002. Nonlinear solid mechanics: a continuum approach for engineering science.

Hughes, T.J., Cottrell, J.A., Bazilevs, Y., 2005. Isogeometric analysis: Cad, finite elements, nurbs, exact geometry and mesh refinement. Computer methods in applied mechanics and engineering 194, 4135–4195.

Kennedy, G.J., Martins, J.R., 2014. A parallel aerostructural optimization framework for aircraft design studies. Structural and Multidisciplinary Optimization 50, 1079–1101.

Kikuchi, N., Oden, J.T., 1988. Contact problems in elasticity: a study of variational inequalities and finite element methods. SIAM.

Klarbring, A., Petersson, J., Rönnqvist, M., 1995. Truss topology optimization including unilateral contact. Journal of optimization theory and applications 87, 1–31.

Lawry, M., Maute, K., 2018. Level set shape and topology optimization of finite strain bilateral contact problems. International Journal for Numerical Methods in Engineering 113, 1340–1369.

Lazarov, B.S., Sigmund, O., 2011. Filters in topology optimization based on helmholtz-type differential equations. International journal for numerical methods in engineering 86, 765–781.

Maute, K., Schwarz, S., Ramm, E., 1998. Adaptive topology optimization of elastoplastic structures. Structural optimization 15, 81–91.

Osher, S.J., Santosa, F., 2001. Level set methods for optimization problems involving geometry and constraints: I. frequencies of a two-density inhomogeneous drum. Journal of Computational Physics 171, 272–288.

Pietrzak, G., Curnier, A., 1999. Large deformation frictional contact mechanics: continuum formulation and augmented lagrangian treatment. Computer methods in applied mechanics and engineering 177, 351–381.

Popp, A., Gee, M.W., Wall, W.A., 2009. A finite deformation mortar contact formulation using a primal–dual active set strategy. International Journal for Numerical Methods in Engineering 79, 1354–1391.

Puso, M.A., Laursen, T.A., 2004. A mortar segment-to-segment contact method for large deformation solid mechanics. Computer methods in applied mechanics and engineering 193, 601–629.

Rozvany, G.I., Zhou, M., Birker, T., 1992. Generalized shape optimization without homogenization. Structural Optimization 4, 250–252.

Scherer, M., Denzer, R., Steinmann, P., 2010. A fictitious energy approach for shape optimization. International Journal for Numerical Methods in Engineering 82, 269–302.

Schmidt, S., Schulz, V., 2011. A 2589 line topology optimization code written for the graphics card. Computing and Visualization in Science 14, 249–256.

Sethian, J.A., Wiegmann, A., 2000. Structural boundary design via level set and immersed interface methods. Journal of computational physics 163, 489–528.

Sigmund, O., Torquato, S., 1997. Design of materials with extreme thermal expansion using a three-phase topology optimization method. Journal of the Mechanics and Physics of Solids 45, 1037–1067.

Simo, J.C., Laursen, T., 1992. An augmented lagrangian treatment of contact problems involving friction. Computers & Structures 42, 97–116.

Simo, J.C., Pister, K.S., 1984. Remarks on rate constitutive equations for finite deformation problems: computational implications. Computer methods in applied mechanics and engineering 46, 201–215.

Sjövall, F., Wallin, M., 2025. A contact aware regularization technique for shape optimization. Computational Mechanics , 1–17.

Sjövall, F., Wallin, M., Tortorelli, D.A., 2024. Shape optimization of hyperelastic structures subject to frictionless contact. Computers & Structures 301, 107426.

Stolpe, M., Svanberg, K., 2001. An alternative interpolation scheme for minimum compliance topology optimization. Structural and Multidisciplinary Optimization 22, 116–124.

Strömberg, N., 2017. Topology optimization of orthotropic elastic design domains with mortar contact conditions, in: World Congress of Structural and Multidisciplinary Optimisation, Springer. pp. 1427–1438.

Strömberg, N., Klarbring, A., 2010. Topology optimization of structures in unilateral contact. Structural and Multidisciplinary Optimization 41, 57–64.

Stupkiewicz, S., Lengiewicz, J., Korelc, J., 2010. Sensitivity analysis for frictional contact problems in the augmented lagrangian formulation. Computer methods in applied mechanics and engineering 199, 2165–2176.

Sukumar, N., Chopp, D.L., Moës, N., Belytschko, T., 2001. Modeling holes and inclusions by level sets in the extended finite-element method. Computer methods in applied mechanics and engineering 190, 6183–6200.

Swartz, K.E., Mittal, K., Schmidt, M., Barrera, J.L., Watts, S., Tortorelli, D.A., 2023. Yet another parameter-free shape optimization method. Structural and Multidisciplinary Optimization 66, 245.

Wadbro, E., Berggren, M., 2006. Topology optimization of an acoustic horn. Computer methods in applied mechanics and engineering 196, 420–436.

Wallin, M., Jönsson, V., Wingren, E., 2016. Topology optimization based on finite strain plasticity. Structural and multidisciplinary optimization 54, 783–793.

Wang, B., Yaylaci, M., Bai, J., Zuo, W., 2025. A 499-line matlab implementation for frictional contact topology optimization. Structural and Multidisciplinary Optimization 68, 1–31.

Wang, C., Zhao, Z., Zhou, M., Sigmund, O., Zhang, X.S., 2021. A comprehensive review of educational articles on structural and multidisciplinary optimization. Structural and Multidisciplinary Optimization 64, 2827–2880.

Wang, M.Y., Wang, X., Guo, D., 2003. A level set method for structural topology optimization. Computer methods in applied mechanics and engineering 192, 227–246.

Wohlmuth, B.I., 2000. A mortar finite element method using dual spaces for the lagrange multiplier. SIAM journal on numerical analysis 38, 989–1012.

Wriggers, P., Korelc, J., Junker, P., 2025. First order finite element formulations for third medium contact. Computational Mechanics , 1–17.

Wriggers, P., Laursen, T.A., 2006. Computational contact mechanics. volume 2. Springer.

Wriggers, P., Schröder, J., Schwarz, A., 2013. A finite element method for contact using a third medium. Computational Mechanics 52, 837–847.

Yang, B., Laursen, T.A., Meng, X., 2005. Two dimensional mortar contact methods for large deformation frictional sliding. International journal for numerical methods in engineering 62, 1183–1225.

Yang, R.J., Chen, C.J., 1996. Stress-based topology optimization. Structural optimization 12, 98–105.

Yoon, G.H., Jensen, J.S., Sigmund, O., 2007. Topology optimization of acoustic–structure interaction problems using a mixed finite element formulation. International journal for numerical methods in engineering 70, 1049–1075.

Zavarise, G., De Lorenzis, L., 2009. The node-to-segment algorithm for 2d frictionless

contact: classical formulation and special cases. Computer Methods in Applied Mechanics and Engineering 198, 3428–3451.

Zienkiewicz, O.C., Campbell, J.S., 1973. Shape optimization and sequential linear programming. Optimum Structural Design .